

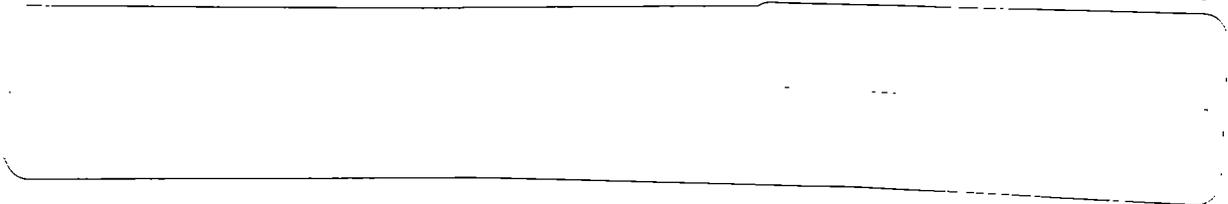
N85-21662



NASA CR 174816



ARC-DRIVEN RAIL GUN RESEARCH



PREPARED FOR
LEWIS RESEARCH CENTER
NATIONAL AERONAUTICS AND SPACE ADMINISTRATION
GRANT NAG 3-76

Annual Report
December 1984



Pradosh K. Ray
Department of Mechanical Engineering
Tuskegee Institute
Tuskegee Institute, Alabama

REPRODUCED BY
U.S. DEPARTMENT OF COMMERCE
NATIONAL TECHNICAL
INFORMATION SERVICE
SPRINGFIELD, VA 22161

1. Report No. NASA CR 174816	2. Government Accession No.	3. Recipient's Catalog No.	
4. Title and Subtitle Arc Driven Rail Gun Research		5. Report Date December 1984	
		6. Performing Organization Code	
7. Author(s) Pradosh K. Ray		8. Performing Organization Report No.	
		10. Work Unit No. YOS 2415 RTOP 506-55-22	
9. Performing Organization Name and Address Mechanical Engineering Department Tuskegee Institute Tuskegee Institute, AL 36088		11. Contract or Grant No. NAG 3-76	
		13. Type of Report and Period Covered Annual Report to Dec., 1984	
12. Sponsoring Agency Name and Address National Aeronautics and Space Administration Lewis Research Center 21000 Brookpark Road Cleveland, OH 44135		14. Sponsoring Agency Code LeRC Code 5323	
		15. Supplementary Notes Grant Monitor: William Kerlake, NASA-Lewis Research Center Cleveland, OH 44135	
16. Abstract <p>The equations describing the performance of an inductively-driven rail gun are analyzed numerically. Friction between the projectile and rails is included through an empirical formulation. The equations are applied to the experiment of Rashleigh and Marshall to obtain an estimate of energy distribution in rail guns as a function of time. The effect of frictional heat dissipation on the bore of the gun is calculated in the experiment of Bauer et al.</p> <p>The mechanism of plasma and projectile acceleration in a dc rail gun is described from a microscopic point of view through the establishment of the Hall field. The plasma conductivity is shown to be a tensor indicating that there is a small component of current parallel to the direction of acceleration. The plasma characteristics are evaluated in the experiment of Bauer et al. as a function of plasma mass through a simple fluid mechanical analysis of the plasma. By equating the energy dissipated in the plasma with the radiation heat loss, the properties of the plasma are determined.</p>			
17. Key Words (Suggested by Author(s)) Rail Gun Electromagnetic Accelerator High-Velocity Projectile Accelerating Plasma		18. Distribution Statement Unclassified--Unlimited	
19. Security Classif. (of this report) Unclassified	20. Security Classif. (of this page) Unclassified	21. No. of Pages 69	22. Price*

* For sale by the National Technical Information Service, Springfield, Virginia 22161

TABLE OF CONTENTS

<u>Topic</u>	<u>Page</u>
Abstract	i
Energy Partitioning in an Inductively-Driven Rail Gun	1
Introduction	1
Rail Gun System	2
Mathematical Formulation	4
Energy Partitioning	10
Results and Discussion	11
Conclusions	18
Nomenclature	20
Friction in Rail Guns	22
Introduction	22
Origin of the Retarding Force	23
Results	23
Dissipation of Energy	24
Conclusion	32
Nomenclature	34
Plasma-Projectile Interaction in an Arc-Driven Rail Gun	35
Introduction	35
Mechanism of Acceleration	36
Plasma Conductivity	39
Characterization of Plasma	42
Induced Magnetic Field	45
Pressure	46
Temperature and Degree of Ionization	48
Density	51
Conductivity and Resistance	51
Results and Discussion	52
Conclusion	58
Nomenclature	61
References	63
Distribution List	65

LIST OF FIGURES

<u>Figure No.</u>	<u>Title</u>	<u>Page</u>
1	Schematic diagram of a rail gun system	5
2	Equivalent lumped-parameter electric circuit	6
3	Acceleration length as a function of time	12
4	Percentage of energy distribution as a function of time	13
5	Effect of accelerator length on projectile exit velocity	15
6	Efficiency and projectile exit velocity as a function of $(L_0/L'X)$	16
7	Plasma resistance and current as a function of time	17
8	Percentage distribution of resistive losses versus time	19
9	Acceleration length as a function of time	25
10	Lorentz force and friction force as a function of acceleration length in the experiment of Bauer et al.	26
11	Lorentz force and friction force versus acceleration length in the experiment of Rashleigh and Marshall	27
12	Frictional energy dissipation as a percentage of total energy delivered to the gun versus acceleration length in the experiment of Bauer et al.	28
13	Charge separation at the edges of plasma due to a magnetic field	37
14	Migration of electrons in the electric and magnetic fields	43
15	Geometry of plasma for modeling	44
16	Variation of pressure along the length of the plasma and average pressure	49

<u>Figure No.</u>	<u>Title</u>	<u>Page</u>
17	Average plasma temperature and average degree of ionization as a function of plasma mass	54
18	Variation of electron and plasma density with the plasma mass	55
19	Effect of variation of plasma mass on plasma length and conductivity	56

LIST OF TABLES

<u>Table No.</u>	<u>Title</u>	<u>Page</u>
1	Input data	9
2	Input data	33
3	Input data for estimating plasma conditions	58
4	Estimated plasma parameters in the experiment of Bauer et al.	59

ENERGY PARTITIONING IN AN
INDUCTIVELY-DRIVEN
RAIL GUN

Introduction

There are a number of applications that require macroparticles moving at very high speeds. Equation of state measurements can be extended with suitable projectile travelling at speeds in excess of 10 km/s [1]. Effects of micrometeoroid impact on space vehicles can be simulated at speeds exceeding 20 km/s [2]. Payloads can be directly launched from the earth's surface to earth orbit or beyond at speeds in the range of 15 to 25 km/s [3] whereas impact fusion might be achievable at speeds greater than 150 km/s [4]. Also there are space propulsion applications [5] and many military applications [6] of projectiles moving at high speeds.

With current technology, projectile speeds in excess of 10 km/s can be obtained only by the use of electromagnetic energy [7]. The simplest of the electromagnetic launching devices is the dc rail gun where the accelerating force is the Lorentz force resulting from a current flowing orthogonally to a self-generated magnetic field. There has been a resurgence of interest in rail guns since Rashleigh and Marshall (hereafter referred to as R & M) successfully accelerated a 3 gm projectile to a velocity of 5.9 km/s in a 5 m long rail gun by using a plasma armature and an intermediate storage inductor for pulse shaping [8]. Inductively-driven rail guns were found to have superior performance characteristics to those

driven with other types of power sources. In the intervening years, a considerable amount of work has been done to explore various aspects of rail gun systems. Limits of rail gun performance have been evaluated by Hawke et al. and velocities up to 10 km/s have been obtained for 3 gm projectiles in a 1.8 m long rail gun [9]. Even so, the experiments by R & M remain one of the most successful ones to date. In this article, the energy partitioning in an inductively-driven rail gun is analyzed as a function of time after the gun is energized and the parameters of R & M experiments are used in this numerical simulation. From a fundamental point of view, the nature of friction between the projectile and rails was found to be rather complex [10]. In view of this, it was explored in this study if the effect of friction on rail gun performance can be adequately expressed through an empirical factor as a function of the velocity of the projectile. This can be shown to be proportional to the square of the projectile velocity. However, a recent study indicated that rail gun performances could be explained by taking into account an increase in the mass of the arc as it ablates materials from the rails [11].

Rail Gun System

The rail gun consists of a pair of parallel conductors separated by a distance and connected by a movable conductor. A large dc current (kilo-amperes) flows in a short burst from one rail to the other through the interconnecting conductor. The interconnecting conductor is normally a thin metallic fuse which becomes a plasma when the large current is discharged through it.

The current flowing in the rails generates a magnetic field B between the rails and this magnetic field interacts with the current flowing in the armature. The resulting Lorentz force $\underline{J} \times \underline{B}$ acting on the armature accelerates the plasma along the rails. If the plasma is confined behind a projectile made of dielectric materials, the pressure of plasma will accelerate the projectile along with the plasma. The confinement of the plasma can be provided by the conducting rails on two sides and dielectric material on the other two sides. During launch operations there are high peaking loads which can be met with a suitable energy storage system. The power sources that are currently being used to supply the primary energy to rail guns include homopolar generator [8], capacitor bank [12] and magnetic flux compression generator [10].

The rail gun functions essentially as a linear dc motor. The plasma behaves as an armature while the parallel rails serve as a single-turn field winding in series with the armature. Hence, the rail gun requires a low voltage, high current power source. The force F acting on the projectile can be represented by

$$F = \frac{L' I^2}{2} \quad (1)$$

Ideally, for constant acceleration a constant current is required and if an inductor is used to deliver the energy to the gun, a close approach to this ideal can be realized [5]. The inductor is also able to overcome the back emf which increases with the increase in velocity of the projectile [6].

A schematic diagram of a rail gun system is shown in Fig. 1. When switches S_1 and S_3 are closed and S_2 is open, a current is generated in the storage inductor from an energy storage device. After the desired current is established in the inductor, switches S_1 and S_3 are opened and S_2 is closed. The projectile is located at the breech of the gun in the beginning, i.e., at $t = 0$, $x = 0$. The fuse at the back of the projectile allows the current to continue to flow until it vaporizes and establishes the arc which accelerates with the projectile along the rails. Just prior to the emergence of the arc from the muzzle of the gun, the switch S_4 is closed to let the current flow through a resistor to extinguish the arc.

Mathematical Formulation

The equations describing the performance of the rail gun are derived by using the conventional lumped-parameter circuit analysis technique. The equivalent electric circuit of a rail gun is shown in Fig. 2. Circuit resistive losses are assumed to be negligible in this analysis.

By applying Kirchoff's law, the differential equation governing the circuit behavior is obtained as

$$\frac{d}{dt} \{(L_0 + L'x)I\} + (R_0 + R'x + R_p)I = 0 \quad (2)$$

$$\text{or, } (L_0 + L'x) \frac{dI}{dt} + (R_0 + R'x + R_p + L' \frac{dx}{dt})I = 0 \quad (3)$$

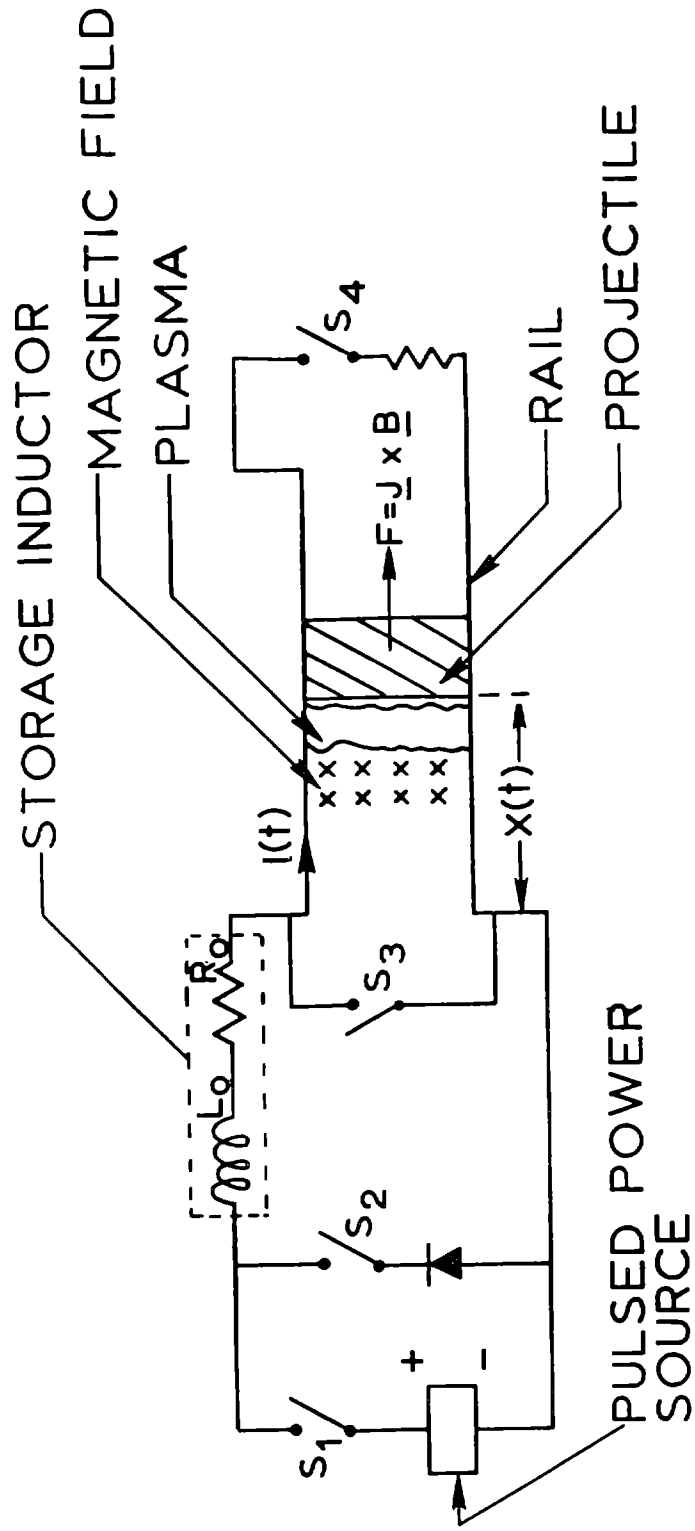


Fig. 1. Schematic diagram of a rail gun system

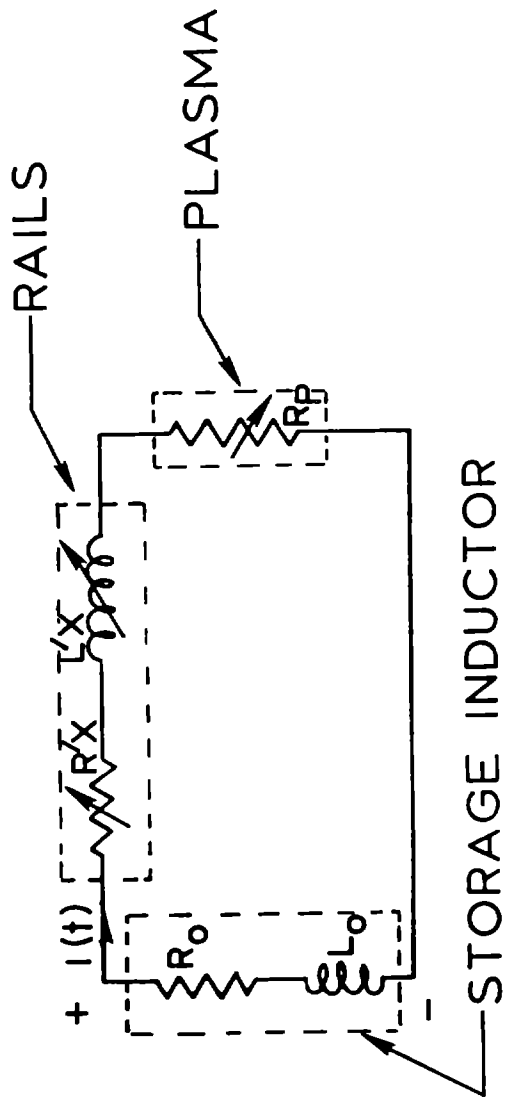


Fig. 2. Equivalent lumped-parameter electric circuit

The motion of the projectile is described by,

$$M \frac{d^2x}{dt^2} = \frac{L'I^2}{2} - F_f \quad (4)$$

The mass of the plasma is neglected as it is much smaller than the mass of the projectile. It is assumed that the friction force can be adequately represented by

$$F_f = bv^n \quad (5)$$

The skin effect confines the current to a thin sheet on the rail surface during the initial part of the acceleration. By assuming a step-current diffusing into a conductor, the skin depth can be represented by [13]

$$\delta(t) = \left(\frac{\pi t}{L\sigma}\right)^{\frac{1}{2}} \quad (6)$$

then,

$$R'(t) = \frac{2}{wD\sigma} \quad (7)$$

where D is equal to the minimum of d or $\delta(t)$.

Equations 3 to 7 represent a highly coupled nonlinear system. The initial conditions are given by

$$\begin{aligned} I(0) &= I_0 \\ x(0) &= 0 \end{aligned} \quad (8)$$

and $\left.\frac{dx}{dt}\right|_{t=0} = 0$

The equations are solved numerically by using a finite difference approximation with a time interval of 20 μ sec. The finite difference equations are,

$$v_{t+\Delta t} = v_t + \frac{L' I_t^2 \Delta t}{2M} - \frac{b}{M} \left(\frac{v_t + v_{t+\Delta t}}{2} \right)^2 \Delta t \quad (9)$$

$$x_{t+\Delta t} = x_t + \left(\frac{v_t + v_{t+\Delta t}}{2} \right) \Delta t \quad (10)$$

$$\delta(t+\Delta t) = \left[\frac{\pi \left(t + \frac{t}{2} \right)}{L\sigma} \right]^{\frac{1}{2}} \quad (11)$$

$$I_{t+\Delta t} = I_t - \frac{L' \left(\frac{v_t + v_{t+\Delta t}}{2} \right) I_t \Delta t + (R_o + R_p + R'_{t+\Delta t} x_{t+\Delta t}) I_t \Delta t}{L_o + L' \left(\frac{x_t + x_{t+\Delta t}}{2} \right)} \quad (12)$$

The value of b and n are adjusted to provide a good fit to the experimental data of R & M. The muzzle voltage of the gun was found to remain constant. Hence, the value of plasma resistance is calculated from

$$R_p(t) = \frac{MV}{I(t)} \quad (13)$$

The values of the parameters used in solving these equations are listed in Table 1. It was found that values of $b = 2.26 \times 10^{-4}$ kg/m and $n = 2$ provide a good fit to the experimental data. The values of b and n can then be used in equation 5 to estimate the friction force.

Table 1
Input Data

Parameter	Value
d	3.2 mm
I_0	300 KA
L_0	22 μ H
L'	0.42 μ H/m
M	3 g
MV	150 volt
R_0	160 μ ohm
X	5 m
t_e	1400 μ sec
V	5.92 km/s
w	12.7 mm
μ	$4\pi \times 10^{-7}$ H/m
σ	0.58×10^8 ohm ⁻¹ -m ⁻¹

Energy Partitioning

At the beginning of the launch cycle, the storage inductor is charged from the primary power supply. When the energy stored in the magnetic field of the storage inductor is delivered to the gun, it is partitioned in four ways;

a) a part of it is dissipated resistively in the rails, in the plasma and in the resistance of the storage inductor,

b) a part of it is stored in the magnetic field of the rails,

c) a part of it is stored in the form of the kinetic energy of the projectile, and

d) a part of it is lost in friction between the rails and the projectile.

Their magnitudes are given by

$$E_r = \int_0^t I^2(t) [R'(t)x + R_p(t) + R_o] dt \quad (14)$$

$$E_i = \int_0^t \frac{L'x}{2} I^2(t) dt \quad (15)$$

$$E_k = \frac{1}{2} Mv^2 \quad (16)$$

and $E_f = E - (E_r + E_i + E_k)$ (17)

where $E = \frac{L_o}{2} (I_o^2 - I_f^2)$ (18)

Results and Discussion

The position of the projectile as a function of time is shown in Fig. 3 in solid line. For comparison, the experimental data points of R & M are shown in solid circles. The theoretical calculation by R & M without friction is also shown in Fig. 3 in broken lines. It is clear that the friction force can be adequately represented by a simple function proportional to the square of the velocity of the projectile.

The energy supplied by the inductor to the gun is shown in Fig. 4 where the percentage of original stored energy remaining in the inductor is plotted against time. It is found that only 37% of the energy of the inductor is supplied to the gun. Also shown in Fig. 4 are the percentage distributions of the delivered energy as a function of time as it is partitioned in four ways. During the initial phase of the acceleration, most of the losses are in resistive heating. The percentages of energy that go to the projectile and to the magnetic field of the rails increase at the beginning, then level off and finally decrease. This indicates an approach to velocity saturation. The energy lost in friction increases monotonically with time. The maximum energy loss occurs in the resistances, amounting to 62% of the total energy supplied by the inductor. At the end of the acceleration, 16% of the energy supplied to the gun remains stored in the magnetic field of the rails, whereas only 15% of the energy is converted into the kinetic energy of the projectile. The frictional loss accounts for the remaining 7% of the energy.

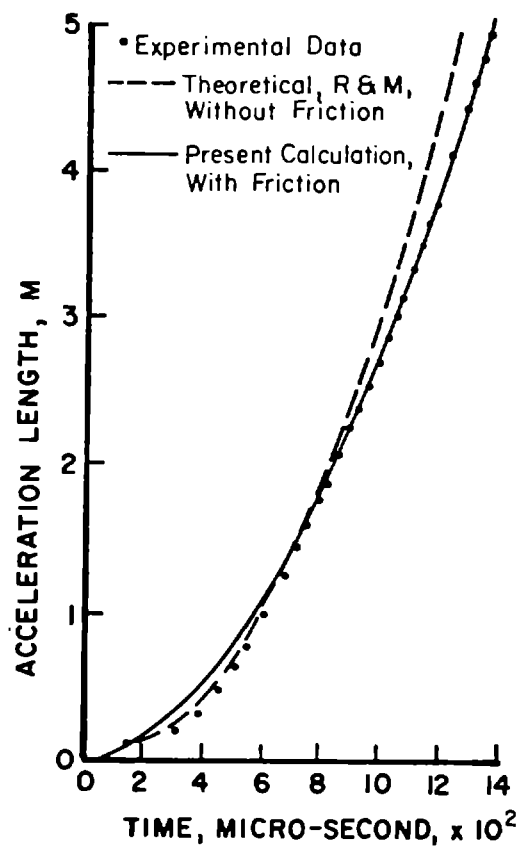


Fig. 3. Acceleration length as a function of time

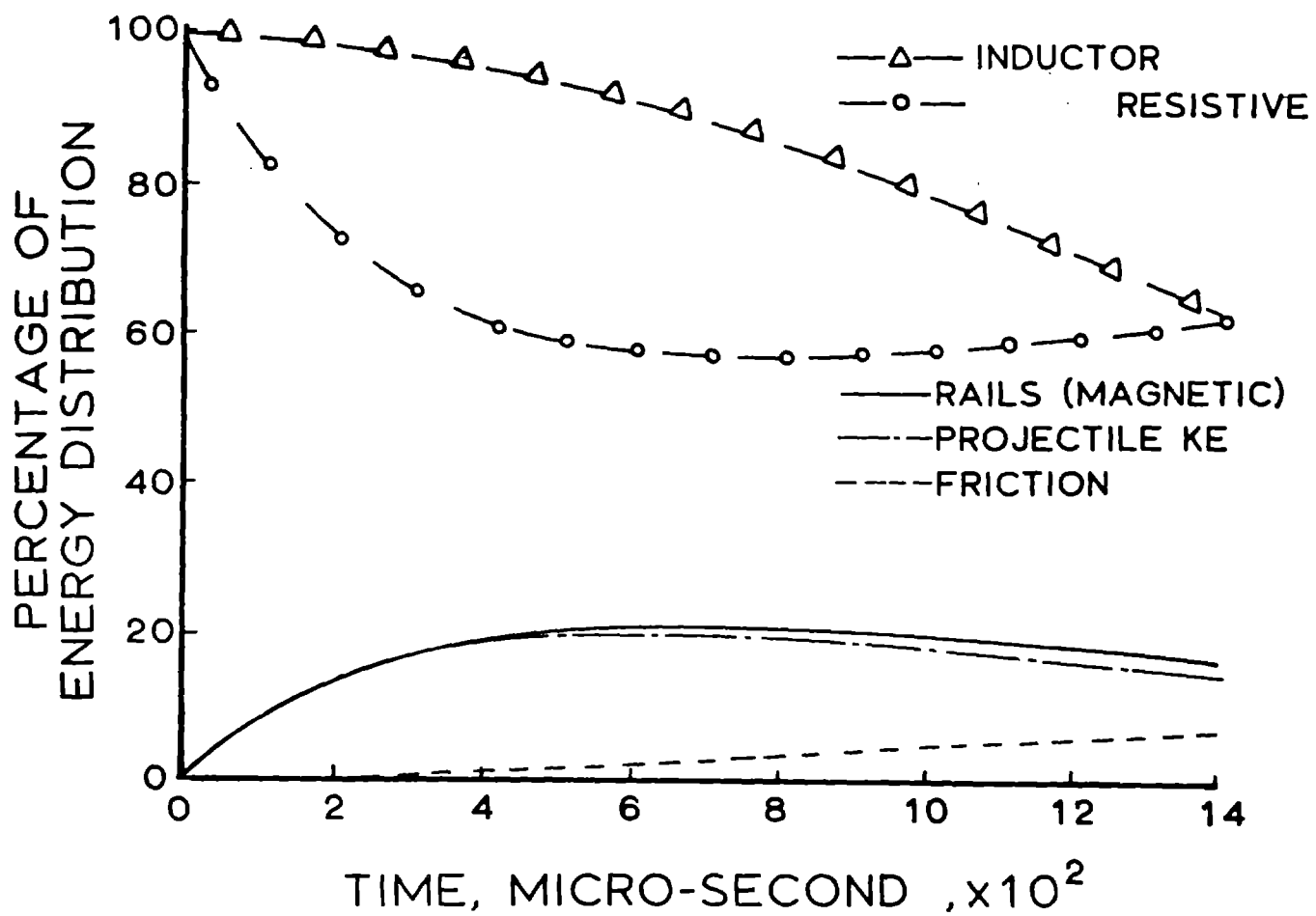


Fig. 4. Percentage of energy distribution as a function of time

The velocity saturation process can be seen clearly in Fig. 5, where the exit velocity of the projectile is plotted against the accelerator length. It is observed that as the accelerator length is increased, the final velocity goes through a maximum, in this case 6.2 km/s.

The efficiency of electric to kinetic energy conversion based on the energy stored in the inductor is only 5.3%. This is due to the fact 63% of the energy stored in the inductor remains undelivered to the gun. Hence, it is desirable to have lower values of L_0 . In Fig. 6, the efficiency of the gun is plotted with respect to $(L_0/L'X)$. It is observed that the efficiency is improved at smaller values of L_0 . However, the exit velocity of the projectile also becomes somewhat smaller at smaller values of L_0 and it starts to saturate at about $(L_0/L'X) = 10$ (Fig. 6). Thus, a compromise has to be made between the efficiency of the rail gun and the final velocity of the projectile.

The current in the gun drops from an initial value of 300 KA to 239 KA (Fig. 7), a decrease of 20%, which has also been observed in the experiments. Correspondingly, the plasma resistance increases from an initial value of 500 μohm to 625 μohm (Fig. 7).

It is found that the current diffuses completely into the rails in 260 μsec . If skin depth is ignored, the total resistive losses at the end of acceleration amount to 55% of the energy supplied by the inductor, as opposed to 62% when skin depth is taken into account.

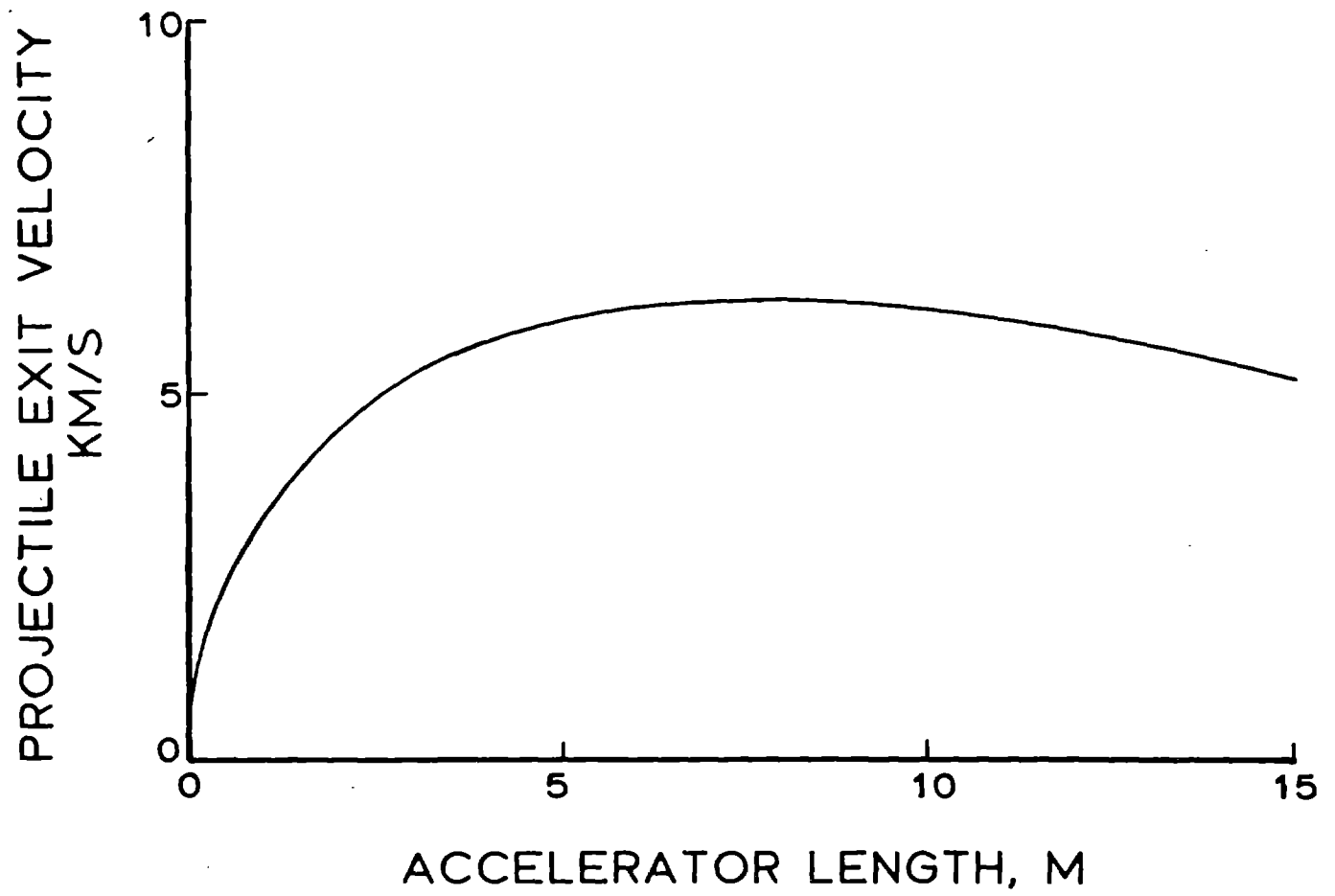


Fig. 5. Effect of accelerator length on projectile exit velocity

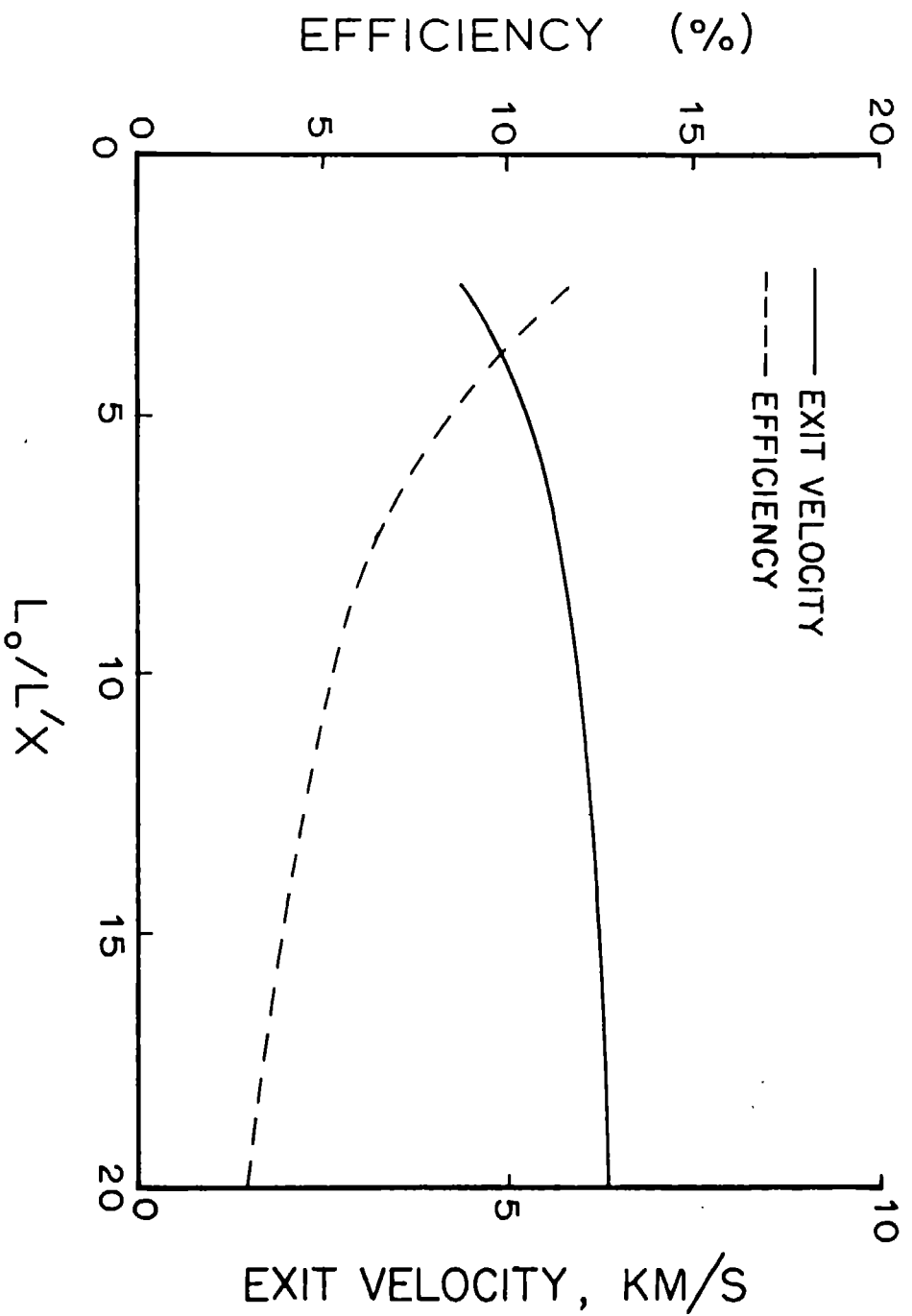


Fig. 6. Efficiency and projectile exit velocity as a function of ($L_0/L'X$)

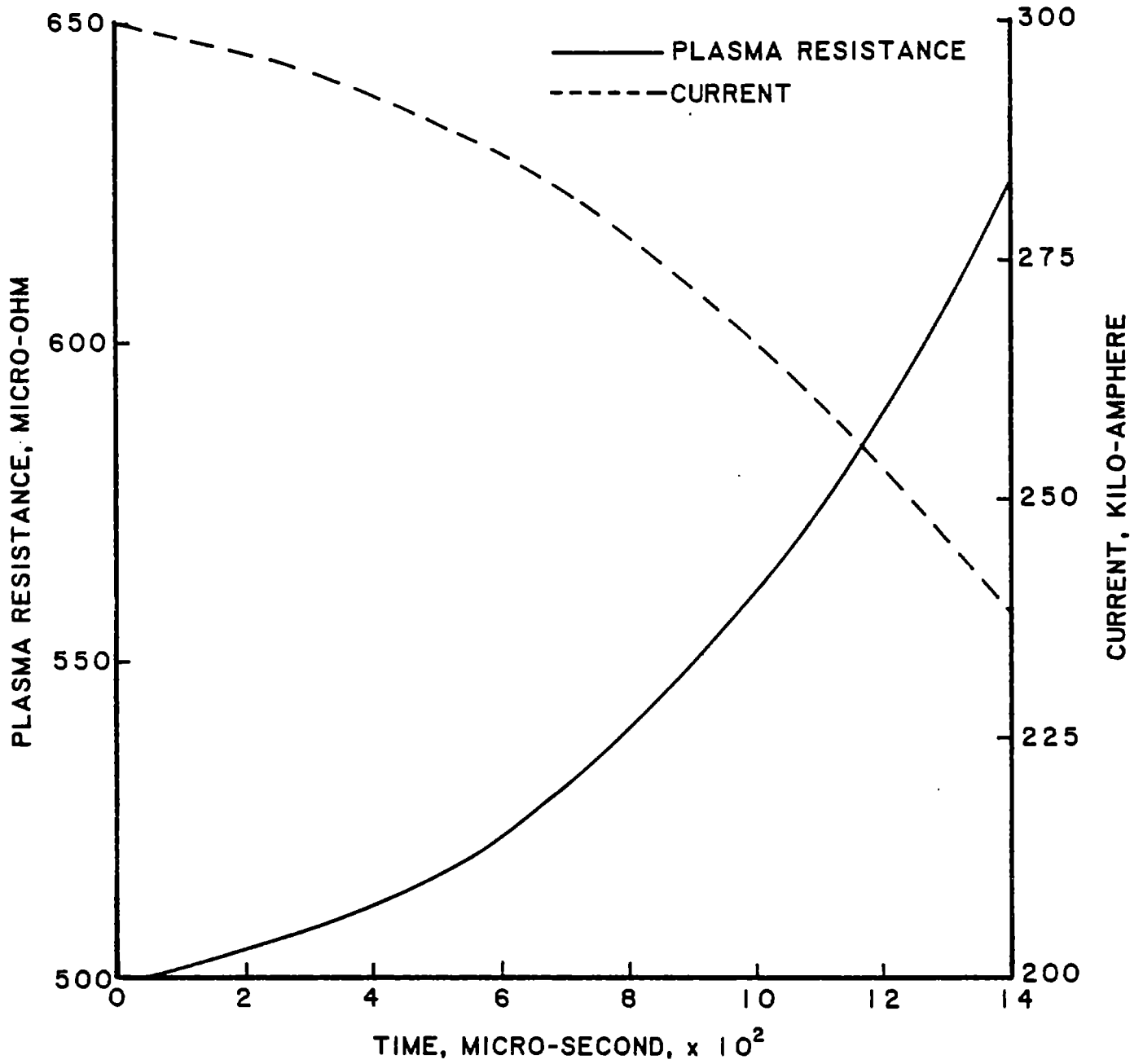


Fig. 7. Plasma resistance and current as a function of time

The resistive losses occur in the rails, in the plasma and in the inductor. The percentage distributions of resistive losses in each of these components are shown in Fig. 8. It is observed that initially the resistive losses in the plasma dominate (~65% of total resistive losses at 200 μ sec) but with time the resistive loss in the rails begins to increase. At the end of acceleration, 85% of total resistive losses occur in the rails.

Conclusions

It is observed that the rail gun is a low efficiency acceleration device. In the experiments of R & M, only 15% of the energy supplied to the gun is transformed into the kinetic energy of the projectile. Much of the energy originally stored in the inductor remains undelivered to the gun although in principle this energy can be recovered. Resistive losses account for the largest amount of energy dissipation and this alone tends to limit the length of the rail guns and hence, the maximum velocity of the projectile.

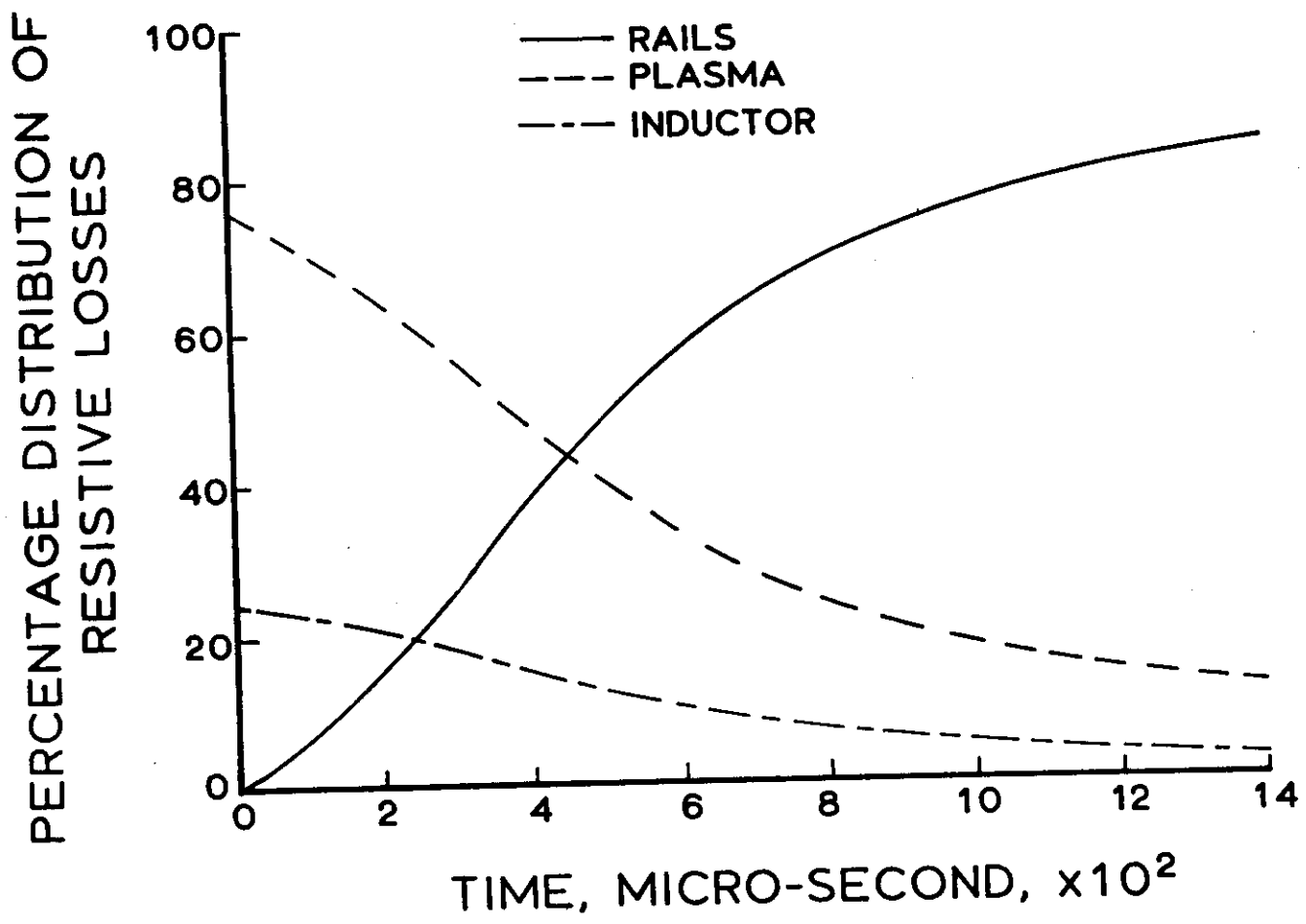


Fig. 8. Percentage distribution of resistive losses versus time

Nomenclature

- b = Proportionality constant for the friction force
- d = Thickness of the rails
- E = Total energy supplied by the inductor
- E_f = Energy lost in friction between the rails and the projectile
- E_i = Energy stored in the magnetic field of the rails
- E_k = Kinetic energy of the projectile
- E_r = Resistive energy loss in the rails
- F = Force on the projectile
- F_f = Friction force
- I = Current in the gun at any time
- I_f = Current in the gun at the end of acceleration
- I_0 = Current in the gun at the beginning of acceleration
- L_0 = Inductance of storage inductor
- L' = Inductance gradient of the rails
- M = Mass of the projectile
- MV = Muzzle voltage
- R_0 = Resistance of the storage inductor
- R_p = Plasma resistance
- R' = Resistance per unit length of the pair of rails
- t = Time
- t_e = Time of exit of the projectile
- v = Velocity of the projectile
- w = Width of the rails
- x = Distance travelled by the projectile
- X = Length of the rail gun

δ = Skin depth

μ = Permeability of the rails

σ = Conductivity of the rails

FRICITION IN RAIL GUNS

Introduction

The velocity of the projectile is theoretically given by

$$v(t) = \frac{L'}{2M} \int_0^t I^2(t') dt' \quad (19)$$

However, rail gun experiments have yielded consistently lower projectile velocities than are to be expected from equation 19. This indicates that the force $F(t) = \frac{1}{2} L' I^2(t)$ is not fully effective in accelerating the projectile. Plasma leakage around the projectile could be partially responsible for this. However, the major cause of reduced acceleration could be due to friction between the projectile and bore surfaces.

Accurate description of these relatively large friction forces in time periods of the order of milliseconds is extremely difficult. As shown earlier, the effect of friction on rail gun performance can be adequately expressed through an empirical formulation as a function proportional to the square of the projectile velocity. It should be noted that semi-empirical formulations are also used in the interior ballistic analysis of conventional chemical propellant driven guns [14].

In this section, the experiment of Bauer et al. is simulated using equations 3 through 13. In this experiment, a 6.3 mm × 3.8 mm × 6.3 mm parallelepiped (0.2 g mass), made of polycarbonate, was accelerated to a velocity of 2 km/s in the first 0.4 m of a 3 m long

gun, when the acceleration of the projectile ceased apparently due to excessive friction between the projectile and the gun [12].

Origin of the Retarding Force

As opposed to the ordinary guns where the projectile base pressure is relatively low, the pressure in the rail gun exceeds the yield strength of the projectile material. Hence, the projectile undergoes plastic deformation and expands against the bore of the gun. The resultant initial contact friction soon gives way to the formation of a multiphase (solid particle and gas) erosive viscous boundary layer where the frictional energy is dissipated [10, 15].

Another source of the retarding force is due to the impulsive loading of the rail gun structure by the magnetic repulsive forces on the rails from the passage of the current. The dynamic stress generated in the structure causes displacements of the rails and the side walls ahead of the projectile [16]. The resultant pinching of the projectile could be severe enough to sufficiently reduce the acceleration of the projectile.

Results

The values of the parameters used in solving the rail gun circuit equations are listed in Table 2. It was found that a value of $b = 8.65 \times 10^{-4}$ kg/m provides a good fit to the experimental data.

The position of the projectile as a function of time is shown in Fig. 9 in solid line. For comparison, the experimental data points of Bauer et al. are shown in this figure in solid circles. The theoretical calculation without friction is also shown in this figure in broken lines.

Figure 10 shows the variation of the Lorentz force and the friction force as a function of the distance travelled by the projectile. The two forces are equal after only 0.4 m of projectile travel. For comparison, the friction force is 66% of the Lorentz force at the muzzle of the gun in Rashleigh and Marshall's experiment (Fig. 11). In the former case, the energy dissipated in friction is 9% of the energy supplied to the gun when the projectile has advanced by 0.4 m from the breech position (Fig. 12). In the latter case, the friction loss amounts to 7% of the total energy delivered to the gun.

Dissipation of Energy

How is the frictional energy dissipated? By taking into account the development of an erosion product, Couette-like viscous boundary layer between the rail and the projectile surface, Buckingham has demonstrated that the projectile will suffer the loss of only a small fraction of its original mass due to dissipation of drag energy [10, 15]. Obviously, the frictional energy has to be dissipated through the rail gun structure.

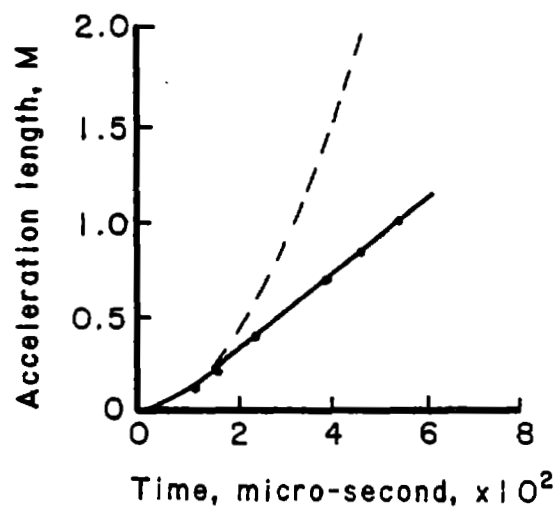


Fig. 9. Acceleration length as a function of time. Solid circles represent experimental data of Bauer et al. [12]. Broken lines represent calculations without friction.

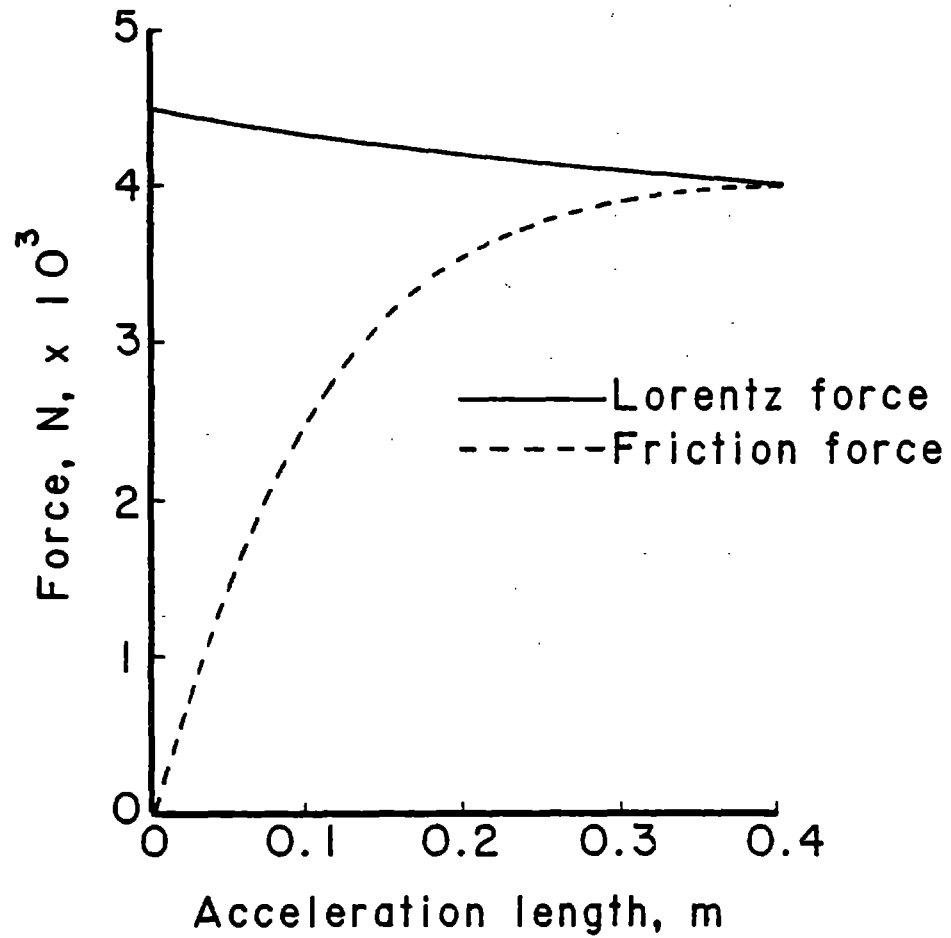


Fig. 10. Lorentz force and friction force as a function of acceleration length in the experiment of Bauer et al.

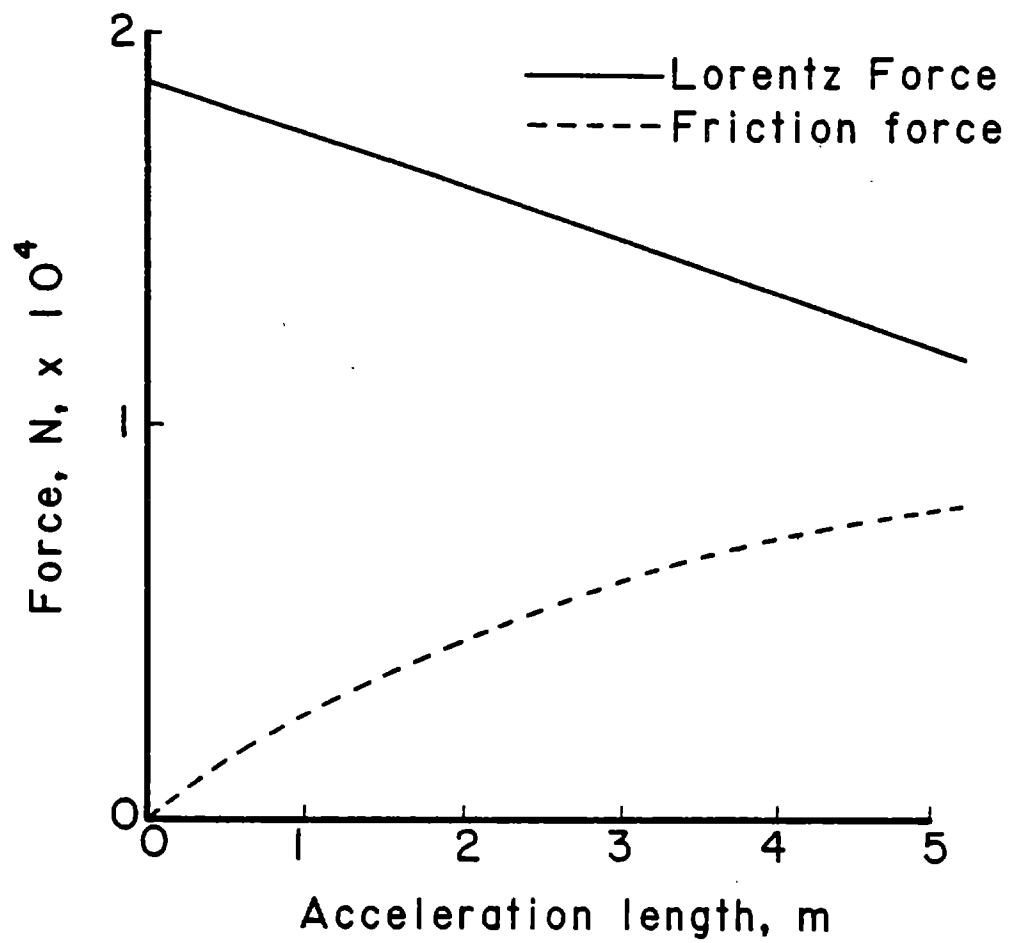


Fig. 11. Lorentz force and friction force versus acceleration length in the experiment of Rashleigh and Marshall

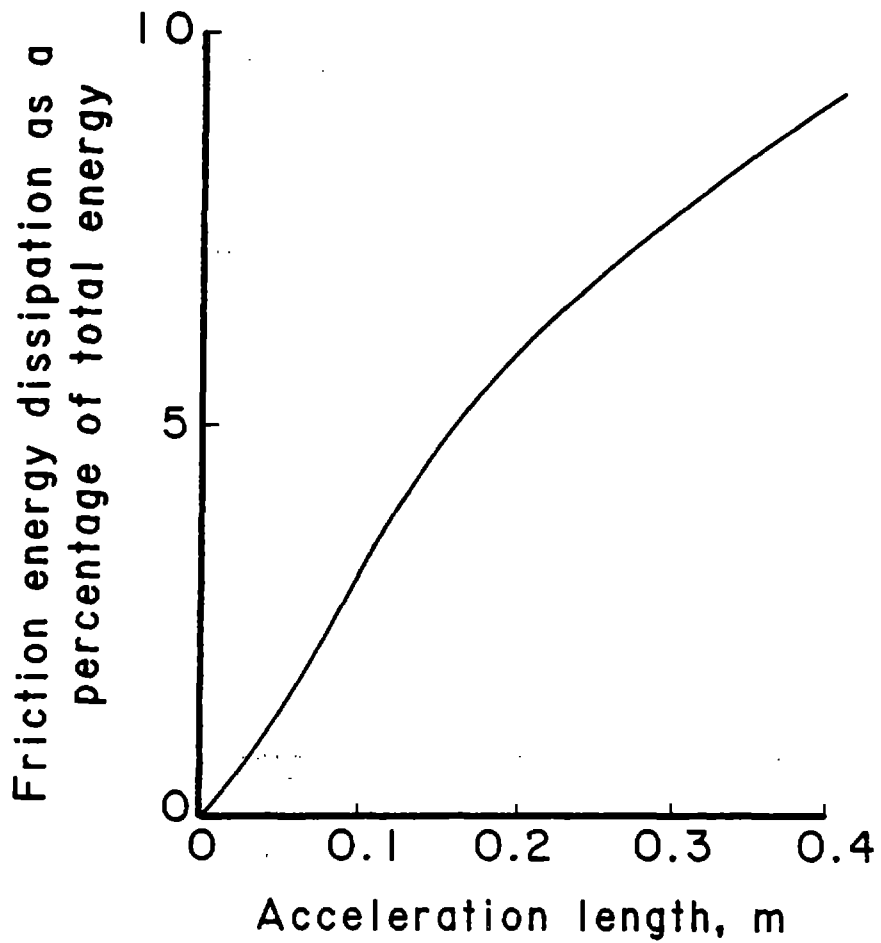


Fig. 12. Frictional energy dissipation as a percentage of total energy delivered to the gun versus acceleration length in the experiment of Bauer et al.

In the experiment of Bauer et al., the projectile ceased to increase in velocity after a short period of acceleration. No significant leakage of plasma to the front of the projectile was detected from the magnetic flux probe measurements. To explain the loss of acceleration, one hypothesis advanced was that the current must have commutated out of the armature into a secondary current path within the launcher. However, no convincing proof was later found to support this hypothesis. Although, it is possible that a small fraction of the current delivered to the gun was shunted from the armature into a spurious path, it is doubtful that the entire current has done so.

The more likely explanation of the loss of acceleration is due to the excessive drag between the projectile and the launcher surfaces. Although the reasons are not entirely clear, small bore rail guns apparently offer more resistances compared to large bore rail guns, as evidenced by the loss of acceleration in other small bore rail gun experiments [17].

The effects of the frictional energy dissipation on the bore surfaces are analyzed in this paper for the experiment of Bauer et al. Only an approximate physical description of the problem is attempted here as the details are too complicated. For this purpose, it is assumed that a quasi-steady state has been established in the projectile rest frame.

When the projectile stopped accelerating, the drag force was estimated to be 4×10^3 N and the projectile velocity was 2×10^3 m/s. If one identifies a specific element of the wall

equal to the length of the projectile in the direction of motion, the energy dissipated in traversing this length is 24 J. This amount of energy by itself is not significantly large (the amount of energy generated in an equivalent length of rail by Joule heating is 8×10^4 J). But, because of the extremely short period of time in which this energy is liberated, the heat flux on the bore surfaces becomes rather large. Assuming that all the frictional energy is uniformly dissipated through the surfaces, the heat flux is found to be 6.5×10^{10} W/m² based on the instantaneous contact area of the projectile with the bore surfaces.

The penetration of heat into a surface can be roughly estimated from

$$\Delta x = (\alpha t)^{\frac{1}{2}} \quad (20)$$

The thermal energy dissipated in time t is $q''t$. Thus, the specific thermal energy of the heated zone is

$$U = \frac{q''t}{\rho(\alpha t)^{\frac{1}{2}}} \quad (21)$$

Conservatively assuming that the heat flux is applied to the surface element for a time period of 3 μ s that it takes the projectile to traverse this length, the specific thermal energy of the copper rails is $U_{Cu} = 1186$ J/g and that of the fiber glass side walls is $U_{glass} = 6.1 \times 10^4$ J/g. Hence the surface of the rails will be raised to a temperature which is beyond the melting point of copper. The glass surfaces will vaporize.

Applying the theory of one dimensional melting of a half-space subjected to a step function heat input at the surface [18]

$$t_m = \frac{\pi k^2 T_m^2}{4\alpha q''^2} \quad (22)$$

The thickness of the zone where the temperature is beyond the melting temperature is given by

$$z_1(t) = \frac{0.16 q''(t-t_m)}{\rho U_m} \quad (23)$$

For the copper rails $t_m \approx 0.5 \mu s$ and $z_1 \approx 5 \mu m$. However, melting is a time-temperature reaction and will occur only under equilibrium conditions. The surface material of the rails is not necessarily molten. Under these conditions, the rail surface is not expected to recede and its temperature will be reduced once the heat source moves beyond the specified surface element.

For the glass side walls, the time for the initiation of vaporization can be calculated by assuming one dimensional heat flow, a continually vaporizing surface with constant heat input at the surface and continued removal of the vaporized material from the surface [19]. Thus

$$t_v = \frac{\pi(k\rho c)(T_v - T_0)^2}{4q''^2} \quad (24)$$

The depth of material removed by vaporization is given by

$$z_2(t) = \frac{q''(t-t_v)}{\rho\{L + c(T_v-T_0)\}} \quad (25)$$

For glass, taking $T_v = 3300^\circ\text{K}$ and $L = 20,000 \text{ J/g}$, one finds $t_v \approx 4 \text{ ns}$ and $z_2 \approx 3.4 \text{ }\mu\text{m}$.

Conclusion

The drag force in a rail gun can be adequately described by an empirical relation $F_f = bv^2$. Obviously, the values of b will depend on the geometry and material composition as well as the structural integrity of the rail gun. No general physical model has yet been developed for friction in this velocity and pressure range to interpret the observed data.

Table 2
Input Data

Parameter	Value
d	6.35 mm
I_0	135 KA
L_0	13 μ H
L'	0.50 μ H/m
M	0.2 g
MV	200 volt
R_0	650 μ ohm
t	250 μ sec
w	6.35 mm
μ	$4\pi \times 10^{-7}$ H/m
σ	0.58×10^8 ohm ⁻¹ -m ⁻¹

Nomenclature

b = Proportionality constant for the friction force

c = Specific heat

F_f = Friction force

I = Current in the rail gun at any time

k = Thermal conductivity

L = Latent heat of vaporization

L' = Inductance gradient of the rails

M = Mass of the projectile

q'' = Heat flux

t = Time

T = Temperature

U = Specific Thermal Energy

v = Velocity of the projectile

z_1 = Thickness of melt

z_2 = Thickness of material vaporized

α = Thermal diffusivity

ρ = Density

Δx = Depth of penetration of heat

Subscripts:

o = Room condition

m = Melting

v = Vaporization

PLASMA-PROJECTILE INTERACTION IN AN ARC-DRIVEN RAIL GUN

Introduction

In a rail gun, the plasma is formed by passing the current through a thin metal foil attached to the base of the projectile. When the inductor is switched into the rail gun circuit, the foil begins to heat up and eventually melts. Since this takes place in a fraction of a microsecond, the physical shape of the foil is maintained by inertia and magnetic pressure. As heat is further added to the still liquid metal by the continuing flow of the current, its temperature rises to the boiling point. However, equilibrium boiling can not take place, so superheating occurs until the liquid metal explodes and forms the plasma. Due to the induced magnetic field and the positioning of the projectile ahead of the foil, the plasma is confined to a finite volume and accelerates together with the projectile. The mechanism of the acceleration process and how the current is partitioned in the plasma are explained in this section.

The characteristics of a rail gun plasma were first studied by McNab for the Rashleigh and Marshall experiment by assuming a steady state and uniform conditions in the plasma [20]. Subsequently, Batteh and Powell calculated plasma properties for a non-uniform plasma in the steady state by using first, one dimensional and later, two dimensional magnetohydrodynamic equations [21, 22]. However, these equations turn out to be very complex and a physical understanding

of the processes that take place in the plasma is not readily achieved. A computer simulation code was developed by Thio where time varying properties of the plasma as a component of the rail gun circuit were evaluated [23]. It was observed recently that the analysis can be considerably simplified by assuming uniform conductivity in the plasma [24]. To gain an insight into the physics of the plasma processes, a simplified analysis is presented here to establish the plasma conditions in the experiment of Bauer et al. by assuming uniform plasma conductivity and by normalizing the pressure, magnetic field and voltage drop across the plasma to the experimental conditions [12].

Mechanism of Acceleration

It is well known from Ampere's law that a conductor carrying a current density \underline{J} in a magnetic field \underline{B} experiences a body force F given by

$$F = \int_{vol} \underline{J} \times \underline{B} \, dV \quad (26)$$

This body force originates from the sum of the Lorentz forces on all the moving charged particles inside the conductor.

The plasma acceleration can be viewed as a simple two step process. The plasma is assumed to be fully ionized. First, due to the passage of the current in the plasma an electric field E_y is set up under which the electrons and the ions acquire drift velocities v_e and v_i respectively ($v_e \gg v_i$). Next, the flow of current generates an induced magnetic field B_z (Fig. 13). Due to this

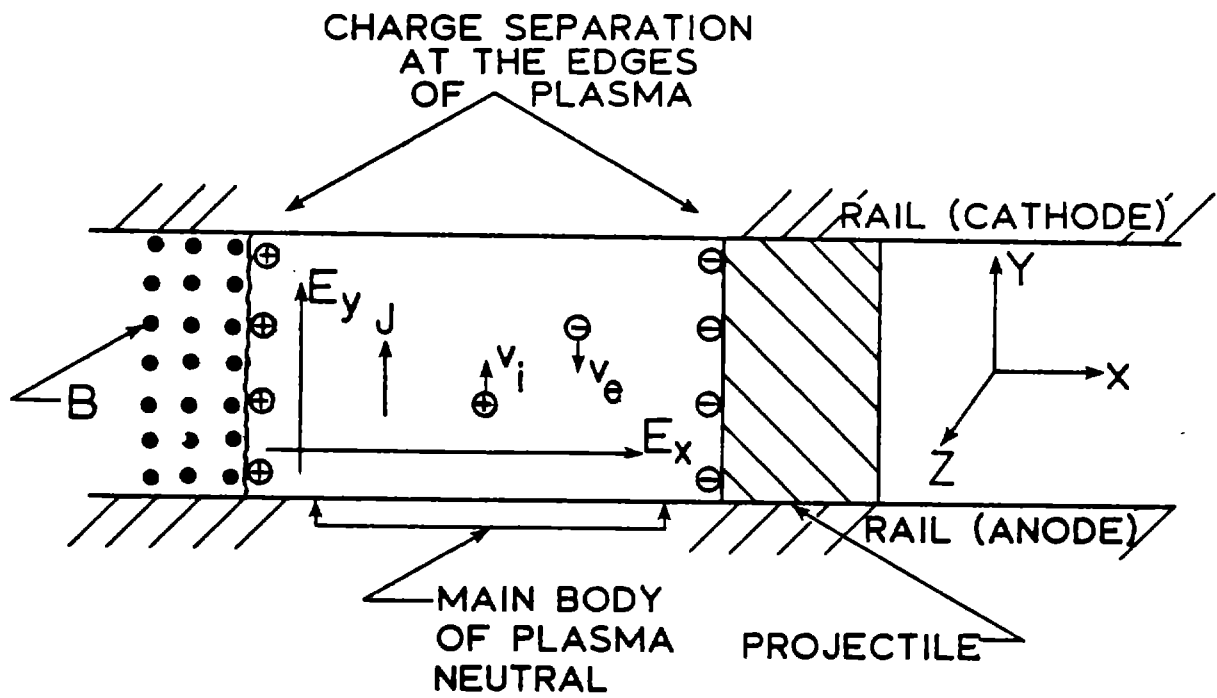


Fig. 13. Charge separation at the edges of plasma due to a magnetic field

magnetic field, the electrons and ions experience Lorentz forces $ev_e B_z$ and $ev_i B_z$ respectively.

The acceleration of the electrons due to the magnetic force is much higher than those of the ions, as the mass of the electrons is much smaller than those of the ions. Thus, an electric charge separation occurs at the plasma boundaries whereas the main body of the plasma remains electrically neutral. The excess electrons at the leading edge of the plasma adhere to the base of the projectile which is made of a dielectric material. Once this is achieved, the charge distribution at the base of the projectile remains fixed and does not move under the influence of any electrical force that may be experienced by it.

Due to the displacement of charges, an electric field E_x (also known as Hall field) is established in the plasma to oppose the separation of charges. Charge separation ceases when the electric force on the electrons is balanced by the magnetic force, i.e.,

$$-eE_x = ev_e B_z \quad (27)$$

However, the ions now experience a net force in the x-direction

$$\begin{aligned} F &= ne(E_x + v_i B_z) \\ &= -ne(v_e - v_i)B_z \end{aligned} \quad (28)$$

The current density J_y is defined by,

$$J_y = -ne(v_e - v_i) \quad (29)$$

Equation 28 then reduces to,

$$F = J_y B_z \quad (30)$$

which is the same as equation 26. But, as soon as the positive ions begin to accelerate, the electrons adhering to the base of the projectile transmit the same force to the projectile to maintain the previously attained charge separation. This makes the plasma and the projectile accelerate together in the rail gun.

Plasma Conductivity

For calculating the conductivity, each constituent species of the plasma is assumed to be a continuous fluid with macroscopic properties derived from appropriate averages over the particles. Thus the plasma is considered to consist of n free electrons, n singly charged positive ions and n_n neutral atoms per unit volume. The neutral atoms are assumed to be coupled to the main body of the plasma through collision processes with electrons and ions.

In the rest frame of the fluid, the electric current is carried predominantly by the electrons. In an ideal, collisionless plasma the charged particles gyrate around the lines of force as they develop drift velocities in the $\underline{E} \times \underline{B}$ direction. In a real plasma, there are collisions between electrons and ions and between electrons and atoms. These collisions produce a damping effect on the motion of the electrons. The damping effect can be expressed by a collision frequency ν_{eT} in terms of the rate at which an electron loses its

momentum through all such collisions. The response of the electrons to the electric and the magnetic field is then determined by the ratio of their gyro frequency ω_e to the collision frequency ν_{eT} . When $\omega_e/\nu_{eT} \ll 1$, as is the case in the rail gun plasmas, the electrons seldom complete one cycle of their drift motion before collision and hence develop little cross field motion.

The average velocity of the electrons \underline{v} in this plasma can be given by the Langevin equation [25, 26]

$$m_e \dot{\underline{v}} = -e(\underline{E} + \underline{v} \times \underline{B}) - m_e \nu_{eT} \underline{v} \quad (31)$$

The flow of electrons corresponds to a current density \underline{J} given by

$$\underline{J} = -ne\underline{v} \quad (32)$$

Substituting the value of \underline{v} from equation 32 into equation 31 and assuming steady state condition one obtains,

$$\begin{aligned} \underline{E} - \frac{1}{ne} \underline{J} \times \underline{B} &= \frac{m_e \nu_{eT}}{ne^2} \underline{J} \\ &= \frac{\underline{J}}{\sigma_0} \end{aligned} \quad (33)$$

$$\text{where } \sigma_0 = \frac{ne^2}{m_e \nu_{eT}} \quad (34)$$

σ_0 can be interpreted as the dc conductivity of the plasma. If the direction of the induced magnetic field is taken as the z-direction, i.e., $\underline{B} = (0,0,B_z)$, equation 33 can be written as

$$\underline{J} = \sigma_0 \underline{E} + \frac{\omega_e}{\nu_{eT}} \underline{J} \times \underline{a}_z \quad (35)$$

$$\text{where } \omega_e = \frac{-eB_z}{m_e} \quad (36)$$

is the electron gyromagnetic frequency and \underline{a}_z is the unit vector in the z-direction. If the electric field in the plasma is given by $\underline{E} = (E_x, E_y, 0)$, then equation 35 can be broken down into its components as

$$J_x - \frac{\omega_e}{\nu_{eT}} J_y = \sigma_0 E_x \quad (37)$$

$$\text{and } \frac{\omega_e}{\nu_{eT}} J_x + J_y = \sigma_0 E_y \quad (38)$$

Equations 37 and 38 can be reduced to

$$J_x = \sigma_{\perp} E_x + \sigma_{\parallel} E_y \quad (39)$$

$$\text{and } J_y = \sigma_{\perp} E_y - \sigma_{\parallel} E_x \quad (40)$$

$$\text{where } \sigma_{\perp} = \frac{\sigma_0 \nu_{eT}^2}{\omega_e^2 + \nu_{eT}^2} \quad (41)$$

$$\text{and } \sigma_{\parallel} = \frac{\sigma_0 \omega_e \nu_{eT}}{\omega_e^2 + \nu_{eT}^2} \quad (42)$$

In the rail guns, $v_{eT} \gg \omega_e$, hence $\sigma_{\parallel} \ll \sigma_{\perp}$. Thus the primary component of the current is parallel to E_y which essentially represents a scalar conduction in the plasma. A small current element is added to it in the perpendicular direction (Fig. 14).

The flow of current in the rail gun can then be represented by

$$\underline{J} = \underline{\sigma} \cdot \underline{E} \quad (43)$$

where $\underline{\sigma}$ is the conductivity tensor and is given by

$$\underline{\sigma} = \begin{bmatrix} \sigma_{\perp} & \sigma_{\parallel} & 0 \\ -\sigma_{\parallel} & \sigma_{\perp} & 0 \\ 0 & 0 & 0 \end{bmatrix} \quad (44)$$

Characterization of Plasma

In the rail gun plasmas $v_{eT} \gg \omega_e$, so the current can be considered to flow in the y-direction only. The plasma conductivity is assumed to be uniform. The assumption of uniform conductivity does not introduce any significant error, but considerably simplifies the calculations [24]. The plasma is considered to be a rectangular parallelepiped of dimension $\ell \times h \times w$ (Fig. 15). It is further assumed that the plasma is singly ionized.

The current density and the current per unit height of the rail are given by

$$J = \frac{I}{\ell h} \quad (45)$$

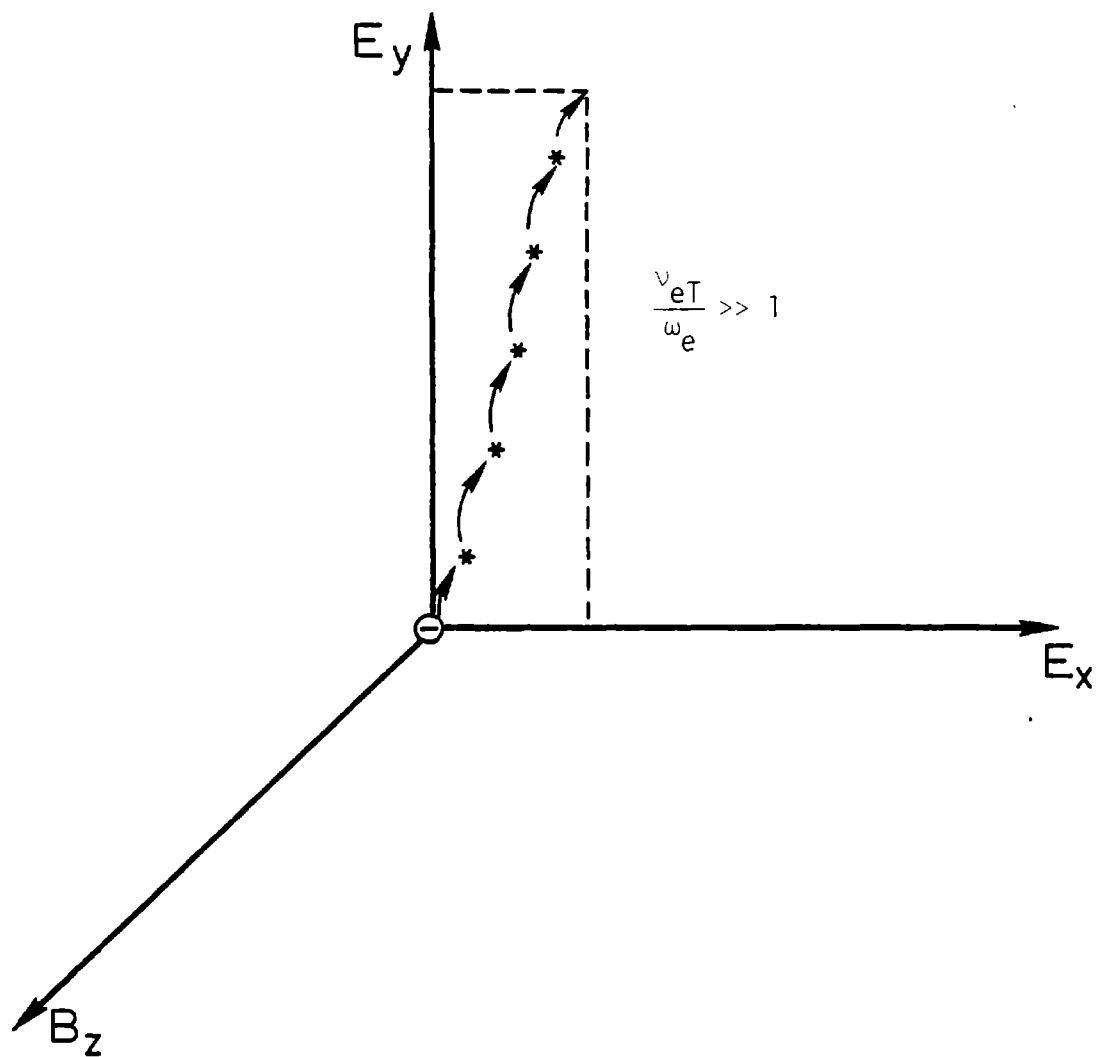


Fig. 14. Migration of electrons in the electric and magnetic fields

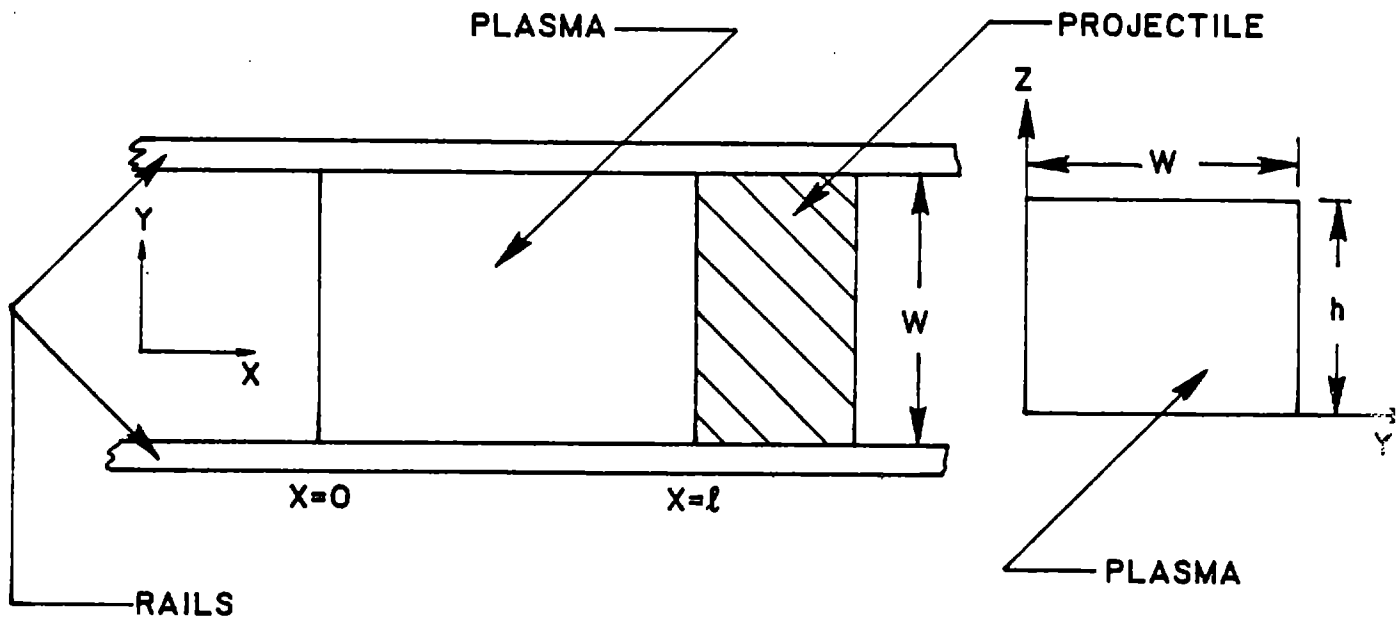


Fig. 15. Geometry of plasma for modeling

and
$$j = \frac{I}{h} \quad (46)$$

Equations 45 and 46 also indicate that

$$J = \frac{j}{\ell} \quad (47)$$

Induced magnetic field

The induced magnetic field \underline{B} can be evaluated from Maxwell's equation

$$\nabla \times \underline{B} = \mu \underline{J} \quad (48)$$

Assuming that the magnetic field varies only in the x-direction, equation 48 reduces to

$$\frac{dB}{dx} = -\mu J \quad (49)$$

At the leading edge of the plasma, the induced magnetic field is zero. With this condition, equation 49 can be integrated to yield

$$B(x) = \mu j \left(1 - \frac{x}{\ell}\right) \quad (50)$$

The magnetic field at the trailing edge of the plasma is then given by

$$\begin{aligned} B(0) &= \mu j \\ &= \frac{\mu I}{h} \end{aligned} \quad (51)$$

However, it was found that this expression overestimates the magnetic field and hence, the propulsive force by a factor of 2 or more, as equation 51 pertains to rails of infinite height [24]. To estimate the value of the magnetic field more accurately, a correction factor f_1 is introduced here, such that

$$B(x) = f_1 \mu j \left(1 - \frac{x}{\ell}\right) \quad (52)$$

The value of f_1 can be found by normalizing the $\underline{J} \times \underline{B}$ force with that calculated from the experimental data. The average magnetic field is then

$$\bar{B} = \frac{f_1 \mu j}{2} \quad (53)$$

Pressure

The pressure in the plasma is assumed to vary in the x-direction. This is a reasonable assumption because pressure will vary significantly in the x-direction only, due to the mechanical effect of the acceleration.

The equation representing the conservation of momentum in the plasma can be written as [27]

$$\rho \frac{du}{dt} + \frac{dP}{dx} = JB \quad (54)$$

Analysis of equation 54 can be considerably simplified by dropping the first term from the equation as it is an order of magnitude

smaller than the electromagnetic body force. Equation 54 then reduces to

$$\frac{dP}{dx} = JB \quad (55)$$

Substituting the values of J and B from equations 47 and 52 into equation 55, one obtains

$$\frac{dP}{dx} = \frac{f_1 \mu j^2}{\ell} \left(1 - \frac{x}{\ell}\right) \quad (56)$$

For a pure electromagnetic acceleration of the plasma, the pressure at the trailing edge is zero. With this condition, equation 56 can be integrated to yield

$$P(x) = \frac{f_1 \mu j^2}{\ell} \left(x - \frac{x^2}{2\ell}\right) \quad (57)$$

The pressure exerted by the plasma at the base of the projectile is then

$$\begin{aligned} P(\ell) &= \frac{f_1 \mu j^2}{2} \\ &= \frac{f_1 \mu I^2}{2h^2} \end{aligned} \quad (58)$$

It has been observed that the force on the projectile at the beginning of acceleration can also be represented by [8]

$$F = \frac{L' I^2}{2} \quad (59)$$

Equating the two forces, one obtains

$$\frac{f_1 \mu I^2}{2h^2} (hw) = \frac{L' I^2}{2} \quad (60)$$

$$\text{giving } f_1 = \frac{L' h}{\mu w} \quad (61)$$

In the experiment of Bauer et al., $h = 3.85$ mm, $w = 6.35$ mm and L' was measured to have a value of $0.5 \mu\text{H/m}$. Substituting these values into equation 61, the value of f_1 is found to be equal to 0.24.

The average pressure is given by

$$\bar{P} = \frac{1}{l} \int_0^l P(x) dx \quad (62)$$

Substituting the value of $P(x)$ from equation 57 into equation 62 and integrating, one obtains

$$\bar{P} = \frac{f_1 \mu j^2}{3} \quad (63)$$

The variation of pressure along the length of the plasma and the average pressure is shown in Fig. 16.

Temperature and degree of ionization

The average temperature of the plasma can be obtained from the average pressure by assuming that the electrons, the ions and the neutral atoms are at the same temperature. This is a reasonable

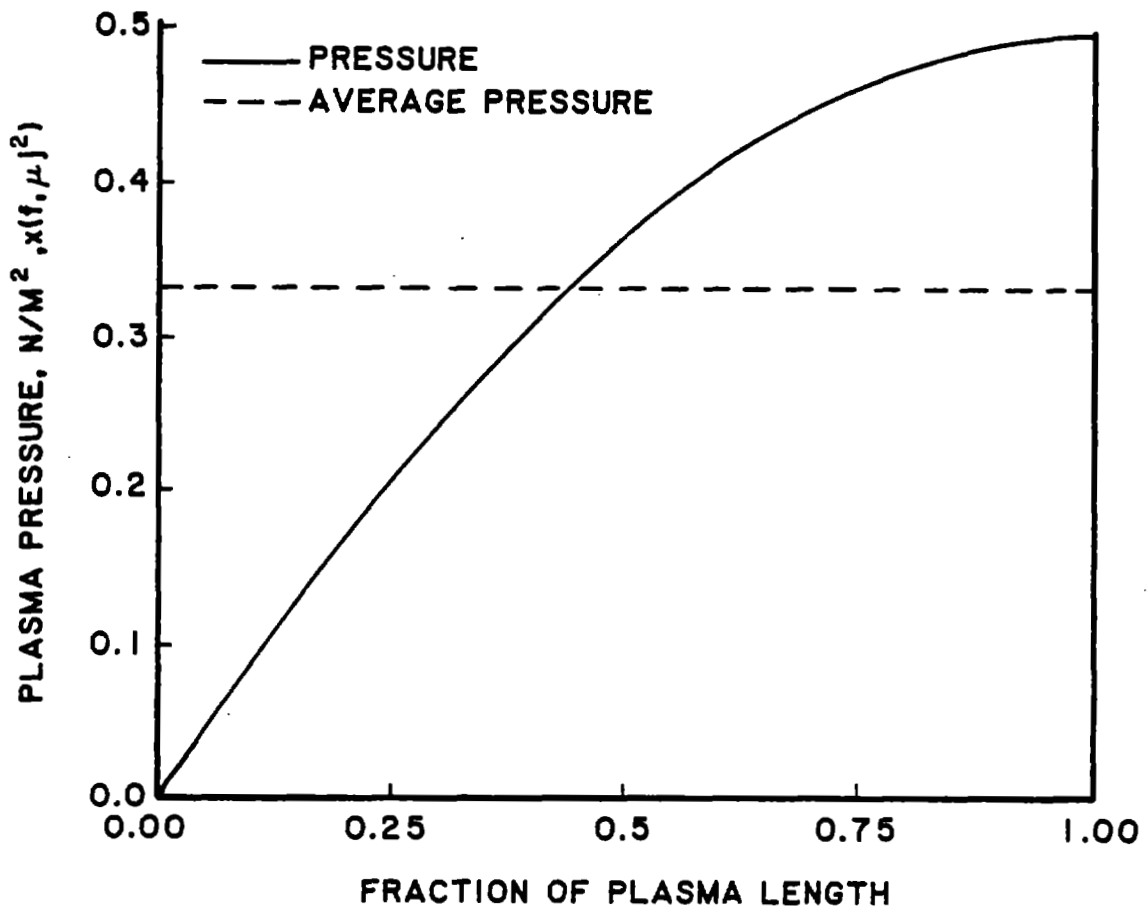


Fig. 16. Variation of pressure along the length of the plasma and average pressure

assumption because due to the high collision frequencies in rail gun plasmas, the time scale in which the particles attain an equilibrium velocity distribution is much smaller than that of the acceleration in the gun. Hence, \bar{P} and T are related by

$$\bar{P} = nkT\left(1 + \frac{1}{\alpha}\right) \quad (64)$$

where α is the average degree of ionization and is defined by

$$\alpha = \frac{n}{n + n_n} \quad (65)$$

The degree of ionization can be obtained from the Saha equation [20]

$$\frac{\alpha^2}{1 - \alpha^2} = \frac{kTK(T)}{\bar{P}} = C \quad (66)$$

where $K(T)$ is given by

$$K(T) = 2.41 \times 10^{21} T^{3/2} \exp\left[\frac{-eV_i}{kT}\right] \quad (67)$$

Thus,

$$\alpha = \left[\frac{C}{1 + C}\right]^{1/2} \quad (68)$$

Density

Neglecting the mass of the electrons, the average density of the plasma is given by

$$\rho = (n + n_n)m_n \quad (69)$$

Substituting the value of α from equation 65 into equation 69, one obtains

$$\rho = \frac{nm_n}{\alpha} \quad (70)$$

Conductivity and resistance

Due to the high collision frequency, the plasma can be assumed to have a scalar conductivity. The plasma conductivity can be calculated from equation 34, where

$$\nu_{eT} = \nu_{ei} + \nu_{en} \quad (71)$$

ν_{ei} and ν_{en} are given by [25]

$$\nu_{ei} = 3.62 \times 10^{-6} n T^{-3/2} \ln \Lambda \quad (72)$$

and
$$\nu_{en} = 2.60 \times 10^{-4} n_n T^{1/2} \quad (73)$$

The Coulomb cutoff parameter Λ represents the extent to which collective plasma effects dominate over individual particle phenomena and is given by [25]

$$\Lambda = 1.23 \times 10^7 T^{3/2} n^{-1/2} \quad (74)$$

The resistance of the plasma is given by

$$R_p = \frac{W}{\sigma_0 \ell h} \quad (75)$$

The length of the plasma is calculated from

$$\ell = \frac{m_p}{\rho h w} \quad (76)$$

The voltage drop across the plasma is

$$V_p = IR_p \quad (77)$$

Results and Discussion

The amount of plasma that is generated from the exploding foil is not determined from the experiments. In view of this, the plasma mass is varied in this study and the parameters that characterize the plasma are evaluated as a function of the plasma mass. The magnetic field and hence, the pressure are of course determined primarily by the current in the rail gun.

The calculations are performed as follows. First, a plasma mass is assumed. Next, the plasma temperature is assumed and the degree of ionization, the plasma density, the electron density, the collision frequency, the plasma conductivity, the plasma length, the plasma resistance and the voltage drop across the plasma are calculated. The calculated voltage drop across the plasma is then checked against the measured muzzle voltage. If the two values are different, a new temperature is selected and the iteration process

is continued until the two values do not differ by more than 1 volt. The plasma mass is then changed to a new value and the whole process is repeated.

In the experiment of Bauer et al., the average mass of the copper foils was approximately 30 mg [28]. In this study, the plasma mass was varied from 10 mg to 50 mg. Figure 17 shows the plasma temperature and degree of ionization as a function of plasma mass. It is observed that the temperature decreases with the increase of plasma mass. Since the voltage drop across the plasma is normalized to the measured muzzle voltage, the plasma resistance remains constant and thus, the ohmic heating in the plasma is constant for a given current. More plasma represents more particles to absorb the energy dissipated in the plasma and hence, the plasma temperature decreases. The degree of ionization of course decreases with an increase in plasma mass as its temperature is lowered.

The variation of electron and plasma density with the plasma mass are shown in Fig. 18. The plasma density increases with plasma mass as the length of the plasma and hence, its volume increases at a much slower rate with the increase of plasma mass (Fig. 19). However, the electron density is initially found to increase and then decrease with an increase in plasma mass. This behavior is due to the fact that the degree of ionization also decreases with the increase of plasma mass. The effect of variation of plasma mass on its conductivity is also shown in Fig. 19. As the plasma mass is increased its temperature decreases which in turn increases the collision frequency. Since collisions represent resistance to the motion of the electrons, an increase

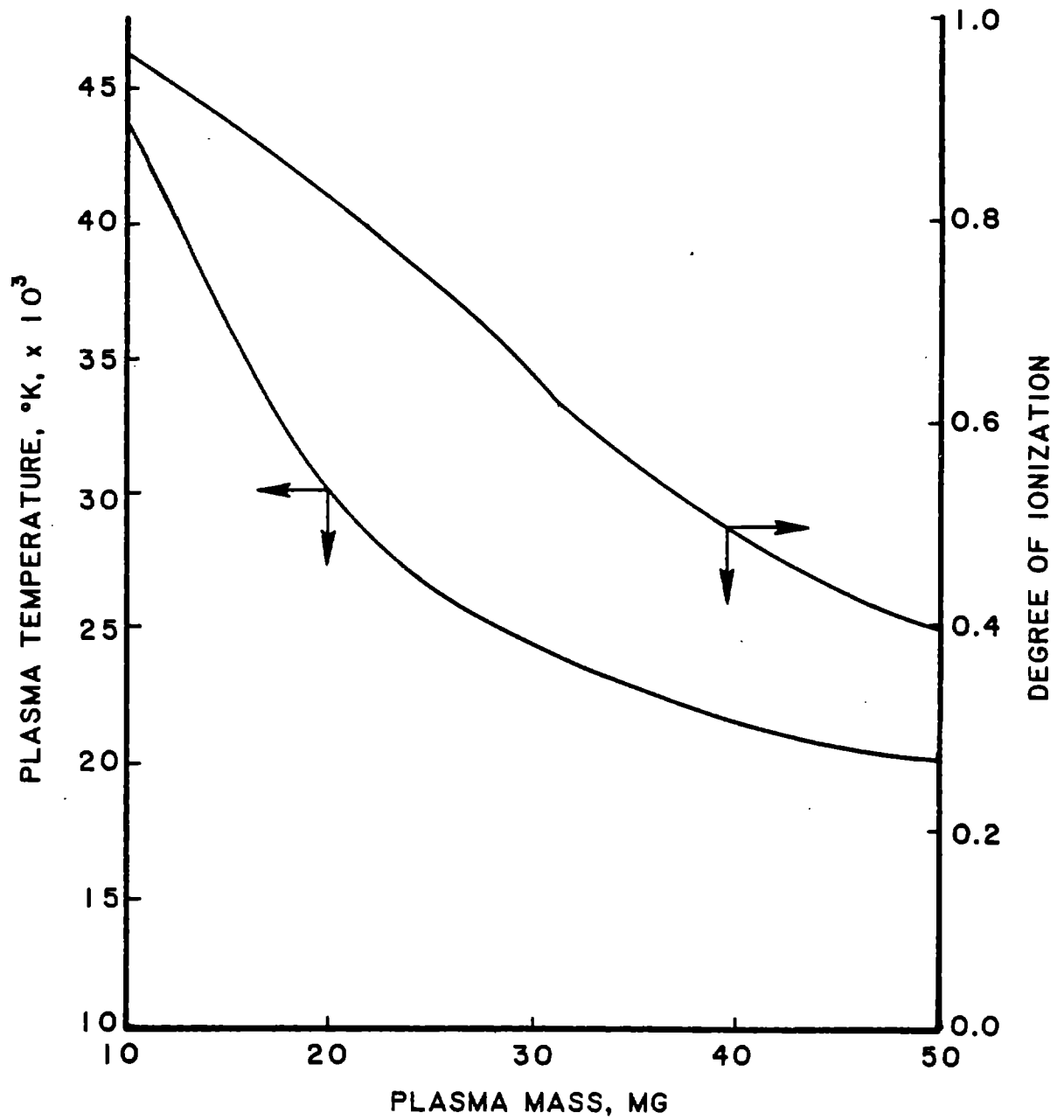


Fig. 17. Average plasma temperature and average degree of ionization as a function of plasma mass

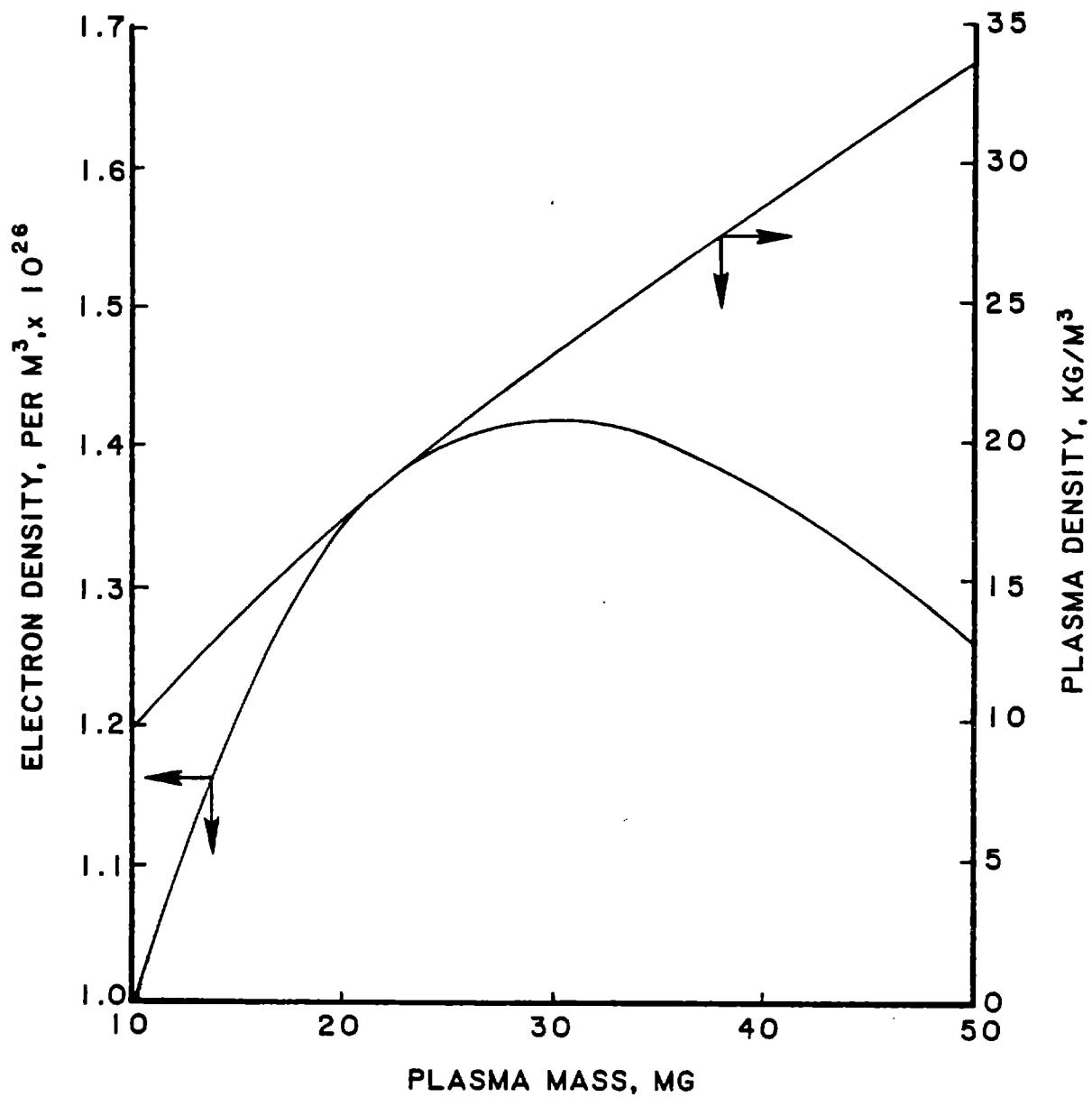


Fig. 18. Variation of electron and plasma density with the plasma mass

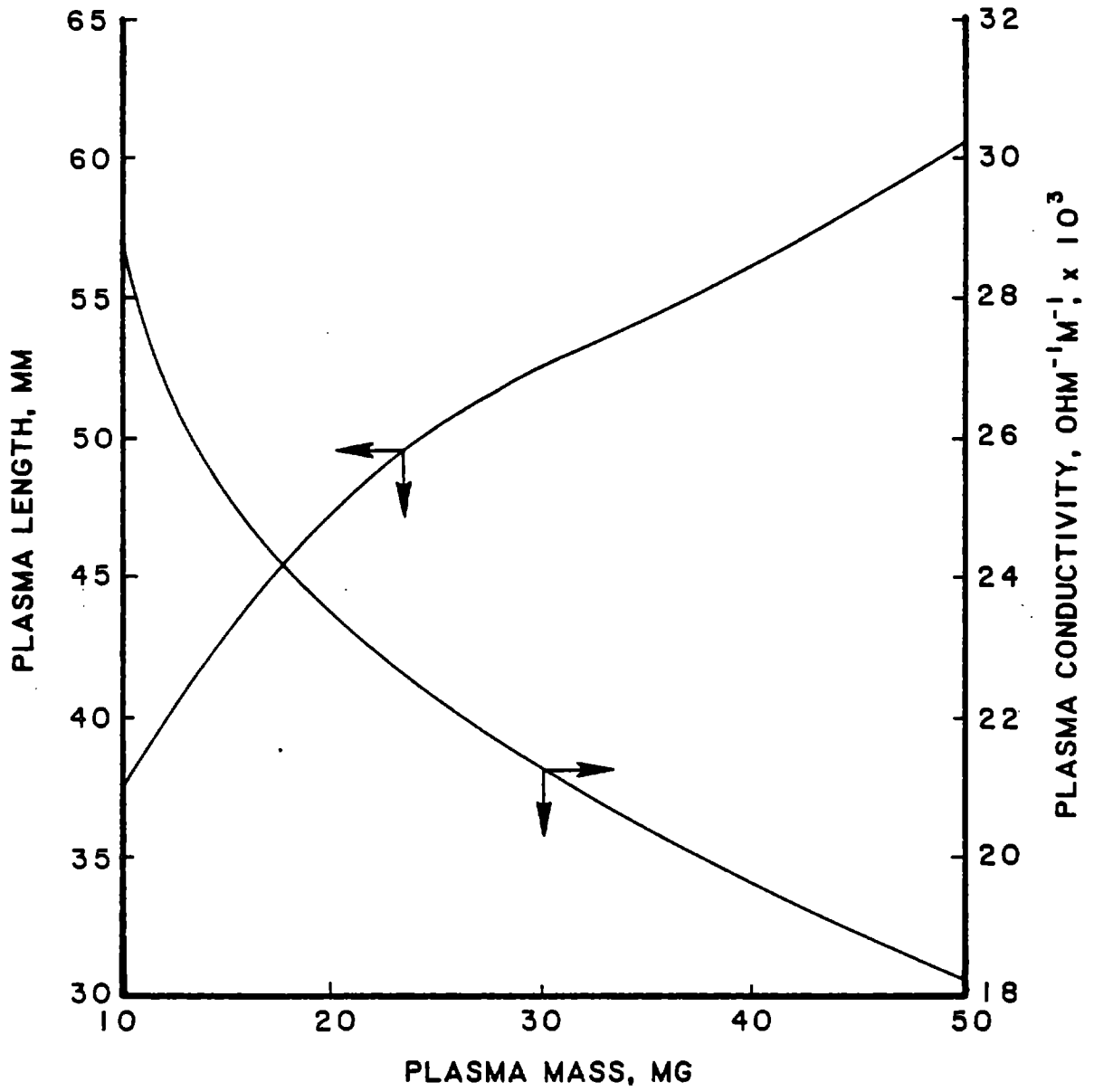


Fig. 19. Effect of variation of plasma mass on plasma length and conductivity

in collision frequency is accompanied with a decrease in conductivity.

Since the actual mass of the plasma could not be determined from the experiment, the plasma conditions can only be estimated. For the plasma to attain an equilibrium condition, the energy dissipated in it by ohmic heating must be balanced by the heat loss from the plasma. Because of the high plasma temperature, the heat loss is primarily by radiation. Thus,

$$I^2 R_p = 2(\omega h + h\lambda + \lambda w)\sigma_s T^4 \quad (78)$$

The temperature obtained from this equation is then matched with the plasma temperature calculated through the iteration process. In this way, the plasma mass and hence, the other plasma parameters can be estimated.

The two temperatures are matched when the plasma mass is 28 mg. This means that over 90 percent of the foil was converted into plasma. More research is needed in the area of exploding foils to determine if such a large portion of the foil can be converted into plasma. Table 3 provides the input data for the experiment of Bauer et al. and in Table 4 the estimated plasma conditions are listed.

The plasma temperature is found to be 25,600°K. This is somewhat lower than the estimate of 44,000 ± 13,000°K by McNab for the plasma in Rashleigh and Marshall's experiment. However, this is expected as equation 78 tends to underestimate the plasma temperature. The plasma is found to be 68% ionized, hence the assumption of singly ionized plasma is justified. The resistance of the plasma

Table 3

Input Data for Estimating Plasma Conditions

Parameter	Value
h	3.85 mm
I	135 KA
L'	0.50 μ H/m
MV	200 volt
w	6.35 mm

is $1.48 \text{ m}\Omega$ and its density is 22.1 kg/m^3 . The length of the plasma is estimated to be 52 mm which is about half the length assumed in McNab's calculations. The electron density is 1.4×10^{26} per m^3 . The ratio of collision frequency to gyromagnetic frequency is 1246, which justifies the assumption of scalar conduction in the plasma.

Conclusion

In a rail gun, charge separation occurs at the edges of the plasma to produce a Hall field. This electric field forces the positive ions and hence, the plasma and the projectile, to accelerate. The plasma conductivity is shown to be a tensor, but because of the high ratio of v_{eT} to ω_e , a scalar conduction in the plasma can be assumed without much error. Plasma properties are estimated as a function of plasma mass through a simple model. It is observed that the magnetic field and hence, the pressure depends on the

Table 4

Estimated Plasma Parameters in the Experiment
of Bauer et al.

Parameter	Value
\bar{B}	5.3 T
j	3.5×10^7 A/m
J	6.8×10^8 A/m ²
ℓ	51.8 mm
m_p	28 mg
n	1.4×10^{26} /m ³
\bar{P}	1.2×10^8 N/m ²
R_p	1.48 m Ω
T	25,600°K
v_e	29.7 m/s
α	0.68
ρ	22.1 kg/m ³
σ_o	21,510 ohm ⁻¹ m ⁻¹
v_{ei}	1.8×10^{14} /sec
v_{en}	4.6×10^{12} /sec
$\frac{v_e T}{\omega_e}$	
ω_e	1,246
$\frac{\sigma_{\perp}}{\sigma_{\parallel}}$	
σ_{\parallel}	198

current in the rail gun. The temperature, the degree of ionization and the plasma conductivity decreases with an increase in plasma mass whereas the plasma density, the plasma length and the electron density increases as the plasma mass is increased. Further study is needed to understand the physics of the processes that take place in an exploding foil so that the plasma mass can be calculated with a high degree of precision.

Nomenclature

\underline{a}_z	= Unit vector in the z-direction
\underline{B}	= Induced magnetic field
\overline{B}	= Average magnetic field
B_z	= Magnetic field in the z-direction
e	= Charge of an electron
\underline{E}	= Electric field
E_x	= Electric field in the x-direction
E_y	= Electric field in the y-direction
f_1	= Correction factor
F	= Force
h	= Height of the rails
I	= Current
j	= Current per unit height of the rail
\underline{J}	= Current density
J_x	= Current density in the x-direction
J_y	= Current density in the y-direction
k	= Boltzmann's constant
ℓ	= Length of the plasma
L'	= Inductance gradient of the rails
m_e	= Mass of electron
m_n	= Mass of neutral atom
m_p	= Mass of plasma
P	= Pressure
\overline{P}	= Average pressure
R_p	= Plasma resistance

t	= Time
T	= Average temperature
u	= Plasma velocity
v, v_e	= Drift velocity of electrons
v_i	= Drift velocity of ions
V_i	= Ionization potential
V_p	= Voltage drop across plasma
w	= Rail separation
α	= Average degree of ionization
δ	= Radius of neutral atom
σ_0	= DC conductivity
$\underline{\underline{g}}$	= Conductivity tensor
ρ	= Average density
μ	= Magnetic permeability
ω_e	= Electron gyromagnetic frequency
ν_{ei}	= Electron-ion collision frequency
ν_{en}	= Electron atom collision frequency
ν_{eT}	= Electron collision frequency, total
Λ	= Coulomb cutoff parameter

REFERENCES

- 1 KREISLER, M.N.: 'How to make things move very fast,' American Scientist, 1982, 70, pp. 70-75
- 2 IGENBERGS, E.B., JEX, D.W., and SHRIVER, E.L.: 'New two-stage accelerator for hypervelocity impact simulation,' AIAA J., 1975, 13, pp. 1024-1030
- 3 KERSLAKE, W.R., and CYBYK, B.Z.: 'Rail accelerator research at Lewis Research Center,' NASA Technical Memorandum 83015, 1982
- 4 RIBE, F.L., and VLASES, G.C.: 'Scope of impact fusion and review of macroparticle accelerators,' Report LA-8000-C, 1979, pp. 1-19
- 5 BARBER, J.P.: 'Electric rail gun application to space propulsion,' AIAA paper no. 79-2091, 1979
- 6 KOLM, H., MONGEAU, P., and WILLIAMS, F.: 'Electromagnetic launchers,' IEEE Trans. Magns., 1980, MAG-16, pp. 719-721
- 7 MARSHALL, R.A.: 'The Australian National University rail gun project,' Atomic Energy, 1975, 1, pp. 16-19
- 8 RASHLEIGH, S.C., and MARSHALL, R.A.: 'Electromagnetic acceleration of macroparticles to high velocities,' J. Appl. Phys., 1978, 49, pp. 2540-2542
- 9 HAWKE, R.S., BROOKS, A.L., DEADRICK, F.J., SCUDDER, J.K., FOWLER, C.M., CAIRD, R.S., and PETERSON, D.R.: 'Results of railgun experiments powered by magnetic flux compression generators,' IEEE Trans. Magns., 1982, MAG-18, pp. 82-93
- 10 BUCKINGHAM, A.C.: 'Electromagnetic propulsion: drag and erosion modeling,' AIAA J., 1981, 19, pp. 1422-1428
- 11 PARKER, J.V.: Communicated by W. R. Kerslake, November, 1984
- 12 BAUER, D.P., MCCORMICK, T.J., and BARBER, J.P.: 'Electric rail gun projectile acceleration to high velocity,' AIAA paper no. 82-1939, 1982
- 13 YOUNG, F.J., HOWLAND, H.R., HUGHES, W.F., and FIKSE, D.A.: 'Interactive electromagnetic launcher simulation,' IEEE Trans. Magns., 1982, MAG-18, pp. 29-32
- 14 BAER, P.G.: 'Practical interior ballistic analysis of guns,' Prog. Astro. Aero., 1979, 66, pp. 37

- 15 BUCKINGHAM, A.C.: 'Projectile and rail launcher design analysis for electromagnetic propulsion to velocities exceeding 10 km/s,' AIAA paper no. 81-0750, 1981
- 16 WANG, S.Y.: 'The structural response of a rail accelerator,' IEEE Trans. Magns., 1984, MAG-20, pp. 356-359
- 17 CLARK, G.A., and BEDFORD, A.J.: 'Performance results of a small-calibre electromagnetic launcher,' IEEE Trans. Magns., 1984, MAG-20, pp. 276-279
- 18 COHEN, M.I.: 'Melting of a half-space subjected to a constant heat input,' J. Franklin Institute, 1967, 283, pp. 271
- 19 LANDAU, H.G.: 'Heat conduction in a melting solid,' Quart. Appl. Math., 1950, 8, pp. 81
- 20 MCNAB, I.R.: 'Electromagnetic macroparticle acceleration by a high pressure plasma,' J. Appl. Phys., 1980, 51, pp. 2549
- 21 POWELL, J.D., and BATTEH, J.H.: 'Plasma dynamics of an arc-driven electromagnetic projectile accelerator,' J. Appl. Phys., 1981, 52, pp. 2717
- 22 POWELL, J.D., and BATTEH, J.H.: 'Two-dimensional plasma model for the arc-driven rail gun,' J. Appl. Phys., 1983, 54, pp. 2242
- 23 THIO, Y.C.: 'PARA: A computer simulation code for plasma driven electromagnetic launchers,' Report no. MRL-R-873, Department of Defense, Australia, 1983
- 24 BATTEH, J.H.: 'Analysis of a rail gun plasma accelerator,' Report no. DAAK11-80-C-0102, Ballistic Research Laboratory, December, 1981
- 25 TANENBAUM, B.S.: 'Plasma Physics,' McGraw-Hill, New York, 1967
- 26 JAHN, R.G.: 'Physics of Electric Propulsion,' McGraw-Hill, New York, 1968
- 27 CHEN, F.F.: 'Introduction to Plasma Physics,' Plenum Press, New York, 1974
- 28 MCCORMICK, T.J.: Private Communication, November, 1984

DISTRIBUTION LIST

	<u>Copies</u>
National Aeronautics and Space Administration Washington, DC 20546	
Attn: RS/Mr. Dell Williams, III	1
RSE/Mr. Van Landingham	1
MT/Mr. Ivan Bekey	1
National Aeronautics and Space Administration Lewis Research Center 21000 Brookpark Road Cleveland, OH 44135	
Attn: Research Support Procurement Section	
Mr. Steve Szabo, MS 501-11	1
Technology Utilization Office, MS 3-19	1
Report Control Office, MS 5-5	1
Library, MS 60-3	2
Dr. M. Goldstein, Chief Scientist, MS 5-3	1
Mr. J. Stone, MS 501-7	1
Mr. D. Byers, MS 501-7	1
Mr. W. Kerslake, MS 501-7	30
Mr. H. Allen, MS 7-3	1
National Aeronautics and Space Administration Lyndon B. Johnson Space Center Houston, TX 77058	
Attn: Mr. Hu Davis	1
National Aeronautics and Space Administration Marshall Space Flight Center Huntsville, AL 35812	
Attn: Mr. George Von Tiesenhausen, P501	1
Mr. Robert Bechtel	1
Research and Technology Division Wright-Patterson AFB, OH 45433	
Attn: (AFWAL/NASA-PO) Mr. Everett Bailey	1
(FTD/TQTD) Capt. David G. Hall	1
NASA Scientific and Technical Information Facility P.O. Box 8757 Baltimore, MD 21240	
Attn: Accessioning Dept.	1

Copies

DARPA/TTO 1400 Wilson Boulevard Arlington, VA 22209 Attn: Dr. Harry D. Fair, Jr.	1
System Planning Corporation ATM Department 1500 Wilson Boulevard Arlington, VA 22209 Attn: Mr. Donald E. Shaw	1
ARDC, AMCCOM Building 382 Dover, NJ 07801 Attn: Dr. Thaddeus Gora Dr. P. J. Kemmey	1 1
U.S. Army ARRADCOM Ballistic Research Lab., DRDAR-BLB Aberdeen Proving Ground, MD 21005 Attn: Dr. Don Ecceshall Dr. J. D. Powell Mr. K. Jamison	1 1 1
USAF Rocket Propulsion Laboratory Edwards AFB, CA 93523 Attn: LKC/Maj. Nordley LKCJ/Dr. Robert Vondra LKCS/Mr. Frank Mead	1 1 1
USAF Armament Lab (AFATL/DLDB) Eglin Air Force Base, FL 32542 Attn: Lt. Richard Walley	1
Boeing Aerospace Co. P.O. Box 3999 Seattle, WA 98124 Attn: Mr. James F. Kenney, MS 8C-23	1
Electromagnetic Launch Research, Inc. 625 Putnam Avenue Cambridge, MA 02139 Attn: Dr. Henry H. Kolm Dr. Peter Mongeau Dr. William Snow	1 1 1
GA Technologies P.O. Box 85608 San Diego, CA 92138 Attn: Dr. Sibley C. Burnett Dr. Michael M. Holland	1 1

Copies

General Dynamics P.O. Box 2507 Pamona, CA 91769 Attn: Mr. J. H. Cuadros	1
General Research Corporation 5383 Hollister Avenue Santa Barbara, CA 93111 Attn: William M. Isbell	1
GT Devices, Inc. 5705 General Washington Drive Alexandria, VA 22312 Attn: Dr. Derek Tidman	1
IAP Research, Inc. 2763 Culver Avenue Dayton, OH 45429-3273 Attn: Dr. John Barber	1
Physics International Company 2700 Merced Street San Leandro, CA 94577 Attn: Dr. Ed Goldman	1
LT Aerospace and Defense Company P.O. Box 225907 Dallas, TX 75265 Attn: Mr. Charles H. Haight	1
Sandia Laboratories P.O. Box 5800 Albuquerque, NM 87115 Attn: Dr. M. Cowan Dr. T. J. Burgess	1 1
Science Applications, Inc. 1503 Johnson Ferry Road Suite 100 Marietta, GA 30067 Attn: Dr. Jad Batteh	1
University of California Lawrence Livermore Lab P.O. Box 805 Livermore, CA 94550 Attn: Dr. Ronald Hawke, L-355	1

Copies

Los Alamos National Scientific Laboratory P.O. Box 1663 Los Alamos, NM 87544 Attn: Dr. J. V. Parker	1
Dr. Max Fowler	1
Dr. Will Fox, MS G787	1
Colorado State University Fort Collins, CO 80521 Attn: Prof. P. J. Wilbur	1
Prof. H. R. Kaufman	1
Westinghouse Electric Corporation 1310 Beulah Road Pittsburgh, PA 15235 Attn: Mr. C. J. Mole	1
Mr. Daniel W. Deis	1
Dr. Y. C. Thio	1
Westinghouse Electric Corporation 401 E. Hendy Avenue Sunnyvale, CA 94088 Attn: Dr. Ian McNab, MS ED-5	1
Mr. Ronald A. Rindal, MS ED-2	1
University of Texas at Austin Center for Electromagnetics Taylor Hall 227 Austin, TX 78712 Attn: Dr. John H. Gully	1
University of Texas at Austin Taylor Hall 167 Austin, TX 78712 Attn: Dr. William E. Weldon	1
Princeton University Princeton, NJ 08540 Attn: Dean R. G. Jahn	1
Dr. Richard A. Marshall P.O. Box 50 Ascot Vale, Victoria 3032 Australia	1
Brookhaven National Lab. Upton, NY 11973 Attn: Dr. James Powell, 802M	1

Copies

BDM Corp. 2227 Drake Ave. Huntsville, AL 35805 Attn: Mr. Steve Mann	1
Mr. Jim Schaaf	1
BDM Corp. One 1st National Plaza, Suite 1010 Dayton, OH 45402 Attn: Mr. Keith J. Maxwell	1
Austin Research Assoc. 1901 Rutland Drive Austin, TX 87858 Attn: Dr. William E. Drummond	1
ASEA AB, Dept. KYEB S-721 83, Vasteras Sweden Attn: Dr. Stefan Toader	1
General Electric Co. ARD No. 3, Plains Road Ballston Spa, NY 12020 Attn: Mr. Wendell Neugebaur	1

